Software Design Document for RAMBHA-DFRS

Prepared by	Lakshmi Jayalal, Keshav R. Tripathi, and Shamayita Ray
Reviewed by	Raj Kumar Choudhary, SPL
Approved by	Raj Kumar Choudhary, PI, RAMBHA-LP

DOCUMENT CONTROL SHEET

01	Security Classification: Unclassified	02	Distribution: Open
03	Document Type: Software Design Document	04	Document : SDD Document
05	Month and Year of Publication : November, 2020	06	Collation : • Pages: 66 • Figures: 36 • Tables: 05 • Appendices: 7
07	Title : Software Design Document for RAMBHA-DFRS LTA Data archiving		
08	Prepared by: Lakshmi Jayalal, Keshav R. Tripathi, and Shamayita Ray		
09	Reviewed by : R. K. Choudhary, PI-DFRS, SPL		
10	Abstract: This document presents the LTA software design for RAMBHA-DFRS.		
11	Keywords: DFRS, LTA		
12	Supplementary element: CCSDS, Blue Book		

CHANGE RECORD

Version		Date	Changed Paragraphs	Remarks
Issue	Revision			
Draft	0	01/10/2020	New document	Initial Draft
Draft	1	17/11/2020	Revised document	Final Draft

CONTENT

LIST OF ACRONYMS

LTA	Long Term Archival
RAMBHA	Radio Anatomy of Moon Bound Hypersensitive Atmosphere and Ionosphere
DFRS	Dual Frequency Radio Science Experiment
SPL	Space Physics Laboratory
VSSC	Vikram Sarabhai Space Centre
.prd	Product File Extension
.obs	Observation File Extension
TTC	Telemetry, Tracking and Command
ISSDC	Indian Space Science Data Centre
RDEF	Raw Data Exchange Format
RO	Radio Occultation
GUI	Graphical User Interface
PS	Postscript

IDL	Interactive Development Language
PLL	Phase Lock Loop
EMXO	Evacuated Miniaturized Crystal Oscillator
CCSDS	The Consultative Committee for Space Data Systems
VCO	Voltage Controlled Oscillator
RF	Radio Frequency

LIST OF TABLES

LIST OF FIGURES

1. INTRODUCTION

This document describes the Software Design Description (SDD) for the Long Term Archival (LTA) of the data from the Radio Anatomy of Moon Bound Hypersensitive Atmosphere and Ionosphere – Dual Frequency Radio Science (RAMBHA-DFRS) experiment onboard Chandrayaan-II. RAMBHA-DFRS is developed at Space Physics Laboratory (SPL) of Vikram Sarabhai Space Centre (VSSC).

2. APPLICATION

The software performs the steps for the calculation of the Doppler shift of the received signal, which is nothing but the deviation in the received frequency as that from the transmitted frequency and the power of the received signal, which can be obtained by using simple Fourier Transform (FT).

The raw input used is the Level 0 – RDEF (Raw Data Exchange Format) data files which contain the product file (*.prd), the observation file (*.obs) and an xml file. The information about the experiment is stored in the *.obs file and .xml file. The information extracted from this file is then used to extract the data from *.prd file and processed to obtain the Doppler shift and power of the signal.

3. REFERENCE DOCUMENTS

RD1	Delta-DOR Raw Data Exchange Format, Recommended Standard, Issue 1, June 2013.
RD2	DFRS paper published in Current Science, 2019

Table 3.1: Reference Documents

4. APPLICABLE DOCUMENT

AD1	DFRS DPSIS Document

Table 4.1: Applicable Documents

5. SCOPE

The software is applicable to the radio occultation experiments. Software produces the calibrated data products and also the corresponding xml files for the PDS4 archival. The xml file follows the standard method of PDS4 archival as given by schema and schmatron. The xml file describes the data file, size and number of records of the data file, the start and stop time of the occultation and the date and time at the time of xml generation.

6. DUAL FREQUENCY RADIO SCIENCE EXPERIMENT (DFRS)

Dual Frequency Radio Science Experiment is a radio science experiment used to analyze the planetary/lunar atmosphere-ionosphere. It uses 2 highly correlated radio frequencies in X-, and S bands. The experiment, as it does not need any specific data to be sent, the signal used for tele-command and ranging can also be used to carry out the said experiment.
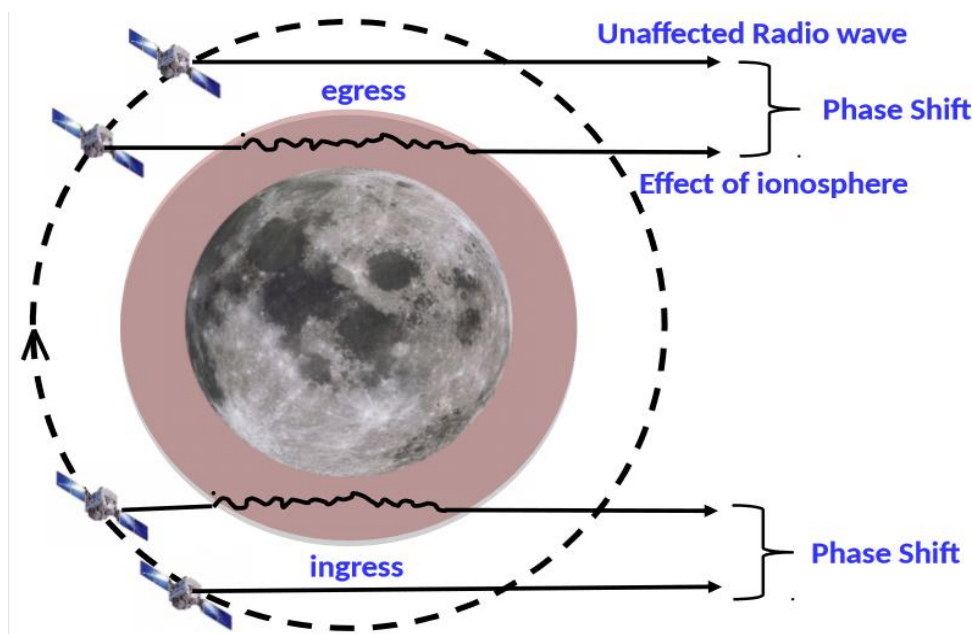
Figure 6.1: Schematic for Radio Occultation

When a radio signal transmitted by a transmitting satellite is obstructed by a celestial object, it is said to be radio occulted. If the body contains an atmosphere - ionosphere then, as the satellite follows its trajectory, before being radio occulted, initial radio signals passes through the ionosphere-atmosphere before reaching the receiver. This period is said to be ingress. The signal is then completely occulted, as a result the receiver will not receive any signal but noises. As the satellite emerges from radio occultation, the signal again passes through the atmosphere-ionosphere of the body before reaching the receiver.

As the signal transverses in the atmosphere of the celestial body, the signal undergoes bending due to the differential refractive index of the atmosphere (Figure 6.1). This bent introduces a path difference in the signal which in-turn introduces a phase shift. Extracting this phase shift from the received signal will help us in understanding the atmosphere of the celestial body.
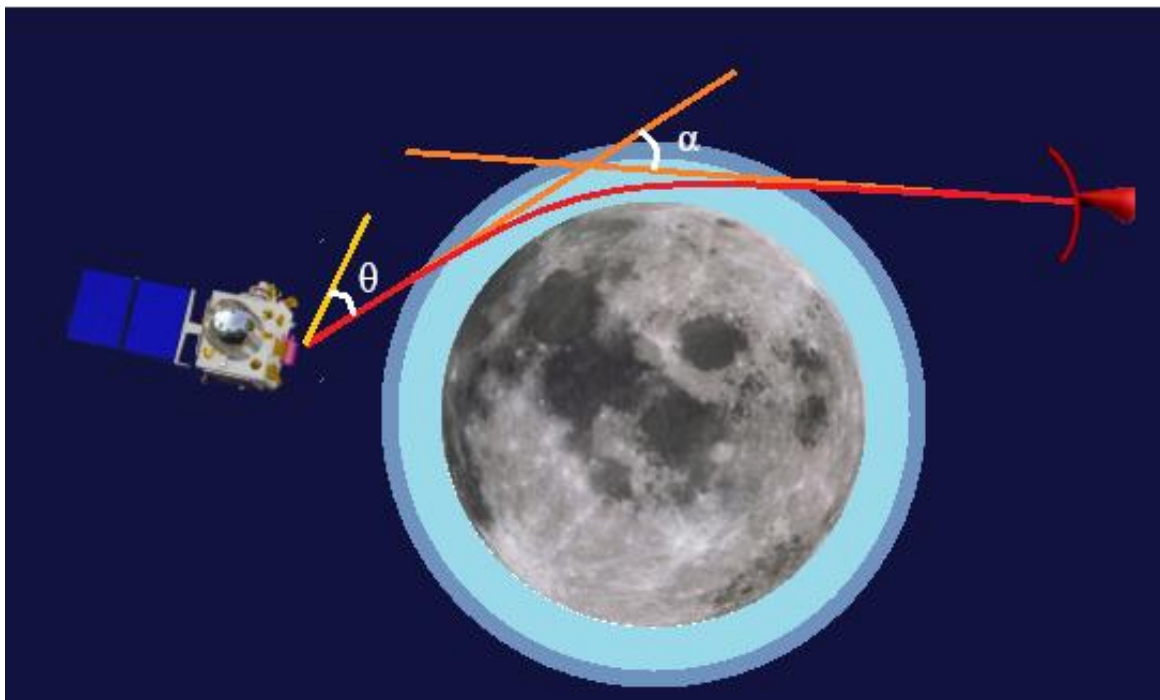
Figure 6.2 : Bending of waves due to the atmosphere of the celestial body

A schematic diagram of Radio occultation experiment is shown in Figure 6.2. In this transmitter on spacecraft is sending radio signal toward receiver. While signal passes through the planetary atmosphere, it deviates from the straight line path. Suppose the 'w' is a

frequency of an electromagnetic wave propagating in the vacuum, with propagation vector 'k' then at any time, the Napierian exponent of the wave would be j(wt -kz). If the wave is passing through the medium with propagation vector 'k_m' then refractive index of the medium would be defined as $\mu_m = k_m/k$. The Napierian exponent in medium can be defined as

$j(wt -k_m z) = j(wt - \mu_m kz)$

$\quad\quad = j (wt -kz + kz - \mu_m kz)$ 　　　　*add and subtract 'kz'*

$\quad\quad\quad = j (wt -kz) +j(kz - (a-jb)*kz)$ 　　*complex refractive index $\mu_m = a - jb$*

$\quad\quad\quad = j(wt -kz) + j(1-a)kz - bkz$

The first term in equation 1 is same as in vacuum, and second term shows variation in the phase, due to the variation of real part of refractive index (a) for given medium. In case of ionosphere the real part of refractive index, a<1 i.e. (1-a) > 0, which implies that signal is gaining phase while passing through the ionosphere. On the other hand, it will suffer phase loss when it passes through the atmosphere, since (a > 1) for neutral atmosphere. Third term in the above equation shows the attenuation (absorption) loss of signal in the medium.

As in the ionosphere phase velocity of the radio signal exceed more than the speed of light which implies that signal will gain the phase and refractive index of the medium will be less than 1 (0.9999976...). This variation in refractive index in cold plasma (temperature less than 1eV) is the function of the frequency of the incident electromagnetic wave and electron density of the plasma medium. The simplified version of Appleton-Hartree equation for dispersive medium can be defined as

$\mu_I = 1 - (40.3*N_e/f^2) *10^6$

where N_e is the number density of electron and f is the frequency of electromagnetic signal.

Deviation of radio signal in neutral atmosphere can be understood by Snell's law of refraction i.e. bending of signal depends on the refractive index of the medium. Retrace the asymptotes of the rays in forward and back direction (as shown in figure 6.2), the interception of these asymptotes will provide the angle of deviation of the signal from its original path. This deviation leads change in the velocity component of signal in direction line receiver. Further this variation in velocity component to atmosphere is incorporated as Atmospheric Doppler (in frequency domain) shift in the signal. Hence increase in refractive index means more

bending, means reduction of velocity in the direction of the observer which implies more atmospheric Doppler. Refractive index of the atmosphere is directly associated with number density and corresponding refractive volume of composition (Eshlemann et al 1973), it's independent of frequency of radio signal.

$$\mu_a = \sum_i K_i n_i$$

where K_i is the refractive volume of ith species and n_i is the number density of that species.

From equation 2 and 3, the electron density of ionosphere and neutral number density of atmosphere can be estimated if refractive index of medium is known. For this experiment, the atmosphere is assumed to be perfectly spherical and that the refractive index is symmetrically uniform for a said layer (i.e. it is dependent on the altitude only). The angle between the asymptotes formed by the bending rays gives the bending angle, α.

The bending angle is a function of Earth's position (considering the planetary center as the origin of the co-ordinate system), position of spacecraft, velocity of spacecraft and the angle between the transmission direction and the velocity of spacecraft (Θ), Figure 6.2.

The Doppler shift is extracted after performing Fourier analysis on the samples. The SPICE files provide the ancillary information such as the spacecraft ephemeris (SPK files), the timing information (LSK and PCK files), reference frames and other parameters relevant to the computation of the occultation geometry. The theoretical Doppler provides the precise information on the contributions of the motion of the spacecraft relative to Earth, and the Earth's atmosphere. The difference of the observed Doppler shift and the theoretical Doppler is the frequency residual: which is the Doppler shift due to the atmosphere and ionosphere of the celestial body.

7. DFRS: Payload and its scientific objectives:

The payload RAMBHA-DFRS aims to study (a) the total electron content (TEC) of the Lunar ionosphere and its morphological changes, (b) quantification of the effect of Earth's magnetosphere and magneto-tail on the production and distribution of plasma in the Lunar Ionosphere, and (c) the altitudinal profiles of the lunar ionosphere. There are two components of this payload, namely (i) observations from Lander to Ground to monitor temporal evolution of the Lunar ionosphere and (ii) observations from Orbiter to Ground in Radio Occultation mode.
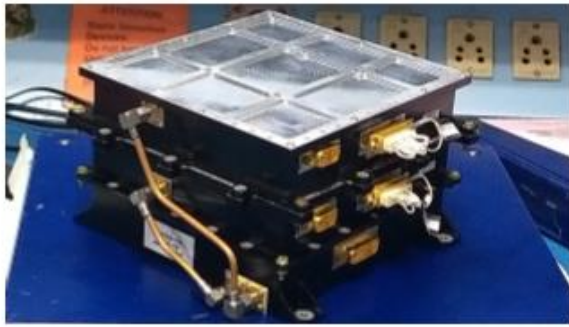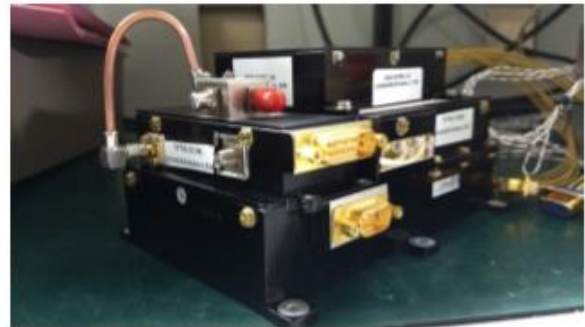
DFRS -10   DFRS -20

Figure 7.1: Flight model version of DFRS-10, and DFRS-20 at Chandrayaan-II

DFRS experiment requires coherent generation of a highly stable carrier in S- and X-Band. To achieve the same, it is required to use a highly stable reference oscillator source for the carrier generation. Thus using Evacuated Miniaturized Crystal Oscillator (EMXO) as a master oscillator to generate radio signal at 20 MHz, which is then further divided to generate coherent dual frequencies at X- and S- band. It provides a short-term stability (Allen Deviation) of better than 10^{-11} in 1 sec with very low power (0.5 W after stabilization) and low mass. To generate the coherent signals, the output of 20 MHz basic EMXO source is fed to a two-way power divider. The two outputs are further fed to the carrier generating circuits using PLL synthesizers, one giving the output at S-band and the other at X-band. Both the carrier generating circuits are similar in function. Carrier is generated directly at the required band using an X-band / S-band VCO and by locking it to the reference EMXO using PLL technique. The carrier at the required frequency is generated by applying appropriate control voltage to VCO from the PLL. The VCO output is passed through a directional coupler whose coupled port output is given to the RF input port of the PLL synthesizer PE97042, the main port output being used as the carrier. A lock status is provided from PLL synthesizer, which is processed to act as the lock indication telemetry. The S-band carrier of frequency 2240MHz is amplified to a level of 26 dBm and is transmitted through a separate S-band patch antenna having a gain of about 2 dBi. The X-band signal is also amplified to a power level of 20 dBm and then applied to the coupled port of a 10 dB directional coupler. The main port of the directional coupler is fed from the X-band Data Transmitter. The frequency of X-band signal for RAMBHA experiment is selected to be 8496 MHz. The combined signal from directional coupler is transmitted through 0.7 m reflector antenna. Hardware is realized as two packages viz. DFRS 10 which houses the X band and S band carrier generators and DFRS 20 which houses the X

band and S band amplifiers. The flight models of DFRS 10, and DFRS 20 are shown in Figure 6.3

8. LTA SOFTWARE DESIGN DESCRIPTION

The software for LTA of DFRS data has been developed in Interactive Data Language (IDL) version 6.3, a programming language used for scientific data analysis. The software is a simple and single ".pro" (.pro is the IDL source code) file, which will be installed at ISSDC in Linux platform. The software has been designed to meet the requirements and is described in the subsequent sections.

9. LTA INPUT AND OUTPUT

The level-0 file in the RDEF format is the raw input for LTA software for RAMBHA-DFRS. RDEF is realized with 3 types of files: an Observation File made of a sequence of ASCII text lines, a Product File made of a sequence of binary data records and an xml file. The Observation File contains information about the radio occultation experiment session for each scan. The Product File contains data collected during a single radio occultation measurement session for a single channel at a single receiver.

The file name uniquely defines the receiver used to record data, the frequency channel, the spacecraft, the station, the scan, the file type, and the nominal scan start time. Each file shall be named according to the following convention:

MMMMnNNNtTsSSSSrRRcCC-YYDDDHHMMSS.XXX

MMMM	The spacecraft ID of the mission
n	token to indicate that scan identifier follows
NNN	scan number per session (three-digit integer) starting from 001
t	token to indicate file type

T	file type; I: Observation file and S: spacecraft scan, Q:quasar scan for the product file
s	token to indicate that station identifier follows
SSSS	station identifier (four characters), which shall be the same as the receiving station name in the Observation File for the given station
r	token to indicate that the receiver identifier follows
RR	receiver identifier
c	token to indicate that channel identifier follows
CC	Channel identifier
-	token to indicate that date follows
YY	the last two digits of the year for nominal scan epoch
DDD	The day of the year for nominal scan epoch
HHMMSS	The hour-minute-second for nominal scan epoch.
.XXX	the file extension: *.obs for an Observation File, *.prd for a Product File.

Table 9.1: Naming Format

9.1 OBSERVATION FILE

The observation file contains the information on each data. There shall be one Observation File for each tracking station and for each measurement session. The Observation File shall be made of a sequence of ASCII text lines.

The Observation File shall contain:

a) a single Observation Header Section, followed by

b) one or more Scan Sections, followed by

c) an Ending Section.

The first character in each line corresponds to the type of information each line contains. 'Z' is used to to indicate the end of each section except for the End of File (EOS) which is indicated by 'E'. Version line starts with 'V', Receiver station by 'R', transmitting station by 'T' (the transmitting station here will be commented as the data transmission is one way. If it's a scan line the first character will be 'S'.

```
# Observation file
V VERSION = 1
# Comments
#
#
R STATION = DS95
# T STATION = NO
Z
#
# SCAN_NUM  SRC_ID      START_TIME      STOP_TIME      RA      DEC      TFREQ
# -------------------------------------------------------------------------------------------------------
S 001       CH2O       2019-276T08:55:00 2019-276T09:13:00 0     0     2296368750.00
#
# DATAFILE                  COH_FLAG     DOR_MULT     FSUB        HARMONIC
# -------------------------------------------------------------------------------------------------------
D CH2On001tSsDS95rR1c01-19276085500.prd    T          1/589      0.000000     0
D CH2On001tSsDS95rR1c02-19276085500.prd    T          1/589      0.000000     0
Z
E *=END=*
```

Figure 9.1: Example of RDEF Observation File

A scan line contains the scan number, source ID, start time and stop time (in YYYY-DDDThh:mm:ss format), right ascension and declination of the source followed by the transmitted frequency.

It shall contain a product line for each channel used. It starts with a 'D' character followed by file name of the *.prd file, a flag to indicate the whether the channels are coherent or not ('T' for True and 'F' for False), a fractional value that needs to be multiplied with the transmitted frequency in case coherent frequencies are used, a subcarrier frequency used when non coherent frequencies are used, a harmonic number of the frequencies used.

Comment in an observation file starts with '#'.

The end line consists of E *=END=*

9.2. PRODUCT FILE

The Product File shall consist of several Records, each one containing exactly one second of data and related information (in Header) to correlate such second of data. Each Record shall consist of data represented in binary format. Each Record shall be made of two Sections,

    a) The Header Section

    b) The Data Section

Each Product File shall contain data for one scan, one channel, and one station. The length of the Header Section is fixed to 176 bits. But the length of the Data Section is variable and is determined by the sample rate and sample size of the recorded data.

.

Figure 9.2: Structure of a product file

The Data Section of each Record of the Product File contains only the in-phase (I) and quadrature-phase (Q) samples recorded at the receiver (I+jQ) . Samples are packed into 32-bit words. The Q data and the I data for a given time sample are adjacent. Between 1 and 16

complex samples shall be packed into each 32-bit word, depending on how many bits per sample are used. The time order of the packed in Little Endian format (i.e. bits are from Least Significant Bit (LSB) to Most Significant Bit (MSB)).

Truncation is used to reduce the number of bits per sample to the desired value. This truncation creates an offset of −0.5 in the output data stream values that needs to be corrected in preprocessing software. To compensate for this offset, each sample shall be put through the transformation $2 \times k + 1$, where k is the 2's complement value of the 1-, 2-, 4-, 8- or 16-bit sample.

This correction gives us an extra bit precision. For example, let i = + 7, the two's complement is k = 0111 since it's positive, take 2 × k, which is just right shift, becomes 01110, adding 1 gives 01111, which is basically 7.5, similarly consider a negative number i = −7, k = 1001, 2 ∗ k + 1 = 10011 which is the two's complement of -7.5.
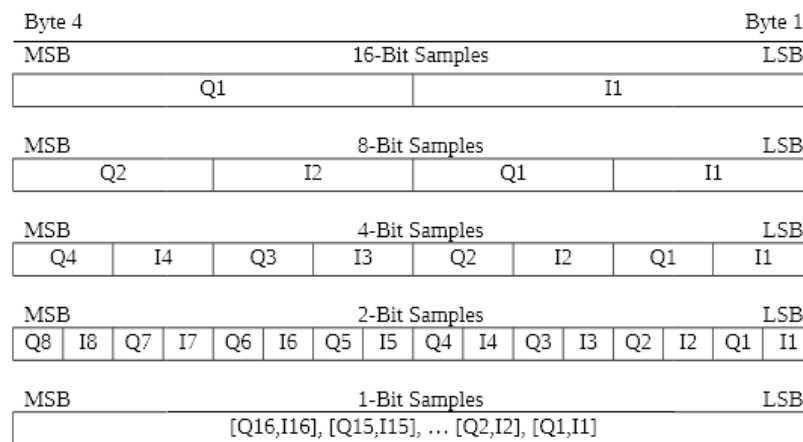

Figure 9.3: All Possible cases for 32- bit word packing

10. SIGNAL PROCESSING

10.1. Processing Platform

On an average, the occultation experiment for this mission lasts for around 1 hour (i.e. 3600 sec) and one record on an average consists of 400000 data points (for a sample rate of 200000)

and 176 header data amounting to 400176 bits per second. Hence, on an average, the product file (*.prd) has a file size of around 1.2 GB. Loading the 1.2 GB data as a whole for programming
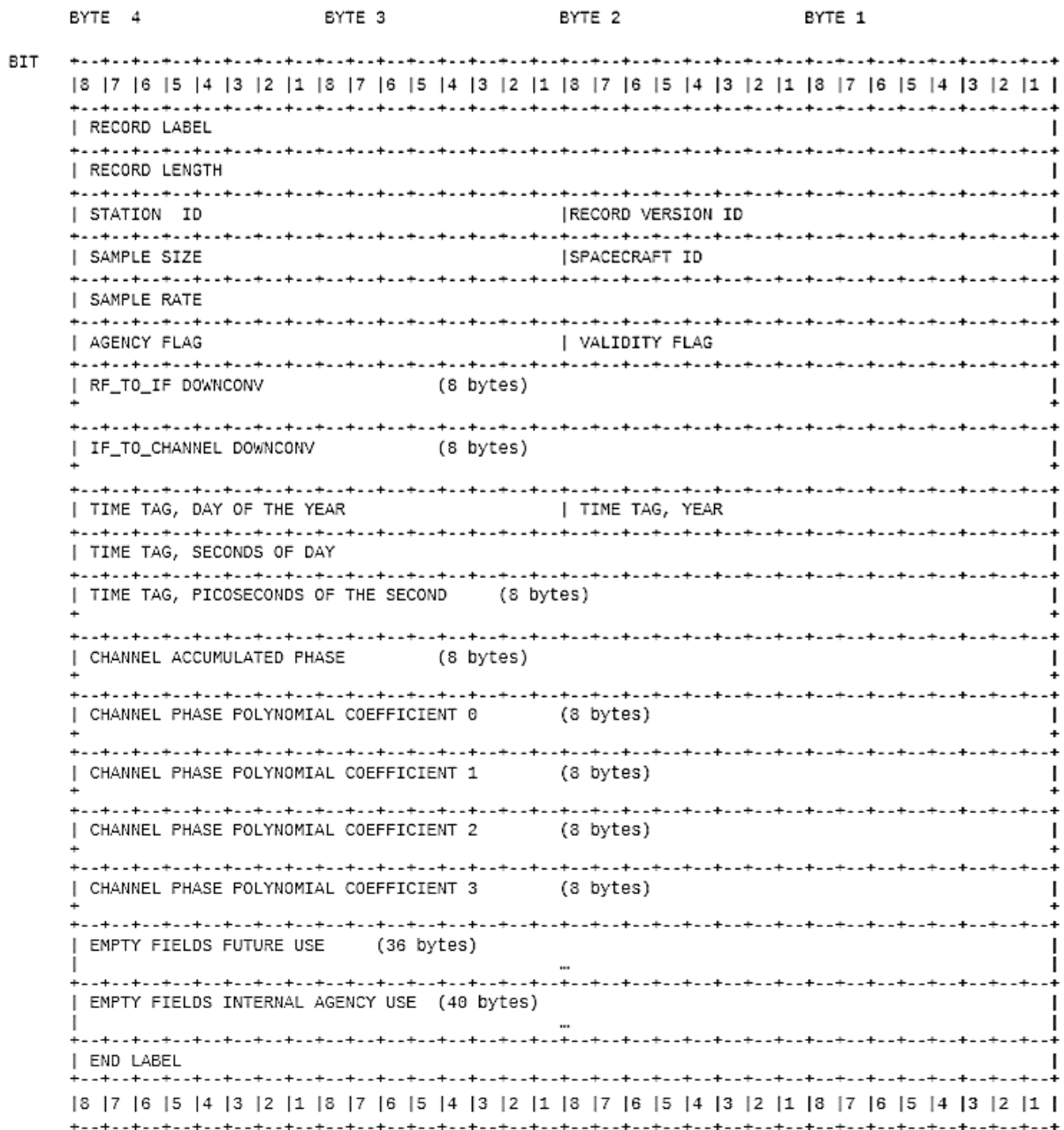
```
       BYTE  4                BYTE 3                BYTE 2                BYTE 1

BIT    +--+--+--+--+--+--+--+--+--+--+--+--+--+--+--+--+--+--+--+--+--+--+--+--+--+--+--+--+--+--+--+--+
       |8 |7 |6 |5 |4 |3 |2 |1 |8 |7 |6 |5 |4 |3 |2 |1 |8 |7 |6 |5 |4 |3 |2 |1 |8 |7 |6 |5 |4 |3 |2 |1 |
       +--+--+--+--+--+--+--+--+--+--+--+--+--+--+--+--+--+--+--+--+--+--+--+--+--+--+--+--+--+--+--+--+
       | RECORD LABEL                                                                                 |
       +--+--+--+--+--+--+--+--+--+--+--+--+--+--+--+--+--+--+--+--+--+--+--+--+--+--+--+--+--+--+--+--+
       | RECORD LENGTH                                                                                |
       +--+--+--+--+--+--+--+--+--+--+--+--+--+--+--+--+--+--+--+--+--+--+--+--+--+--+--+--+--+--+--+--+
       | STATION  ID                              |RECORD VERSION ID                                  |
       +--+--+--+--+--+--+--+--+--+--+--+--+--+--+--+--+--+--+--+--+--+--+--+--+--+--+--+--+--+--+--+--+
       | SAMPLE SIZE                              |SPACECRAFT ID                                      |
       +--+--+--+--+--+--+--+--+--+--+--+--+--+--+--+--+--+--+--+--+--+--+--+--+--+--+--+--+--+--+--+--+
       | SAMPLE RATE                                                                                  |
       +--+--+--+--+--+--+--+--+--+--+--+--+--+--+--+--+--+--+--+--+--+--+--+--+--+--+--+--+--+--+--+--+
       | AGENCY FLAG                              | VALIDITY FLAG                                     |
       +--+--+--+--+--+--+--+--+--+--+--+--+--+--+--+--+--+--+--+--+--+--+--+--+--+--+--+--+--+--+--+--+
       | RF_TO_IF DOWNCONV              (8 bytes)                                                      |
       +                                                                                              +
       +--+--+--+--+--+--+--+--+--+--+--+--+--+--+--+--+--+--+--+--+--+--+--+--+--+--+--+--+--+--+--+--+
       | IF_TO_CHANNEL DOWNCONV         (8 bytes)                                                      |
       +                                                                                              +
       +--+--+--+--+--+--+--+--+--+--+--+--+--+--+--+--+--+--+--+--+--+--+--+--+--+--+--+--+--+--+--+--+
       | TIME TAG, DAY OF THE YEAR                | TIME TAG, YEAR                                    |
       +--+--+--+--+--+--+--+--+--+--+--+--+--+--+--+--+--+--+--+--+--+--+--+--+--+--+--+--+--+--+--+--+
       | TIME TAG, SECONDS OF DAY                                                                     |
       +--+--+--+--+--+--+--+--+--+--+--+--+--+--+--+--+--+--+--+--+--+--+--+--+--+--+--+--+--+--+--+--+
       | TIME TAG, PICOSECONDS OF THE SECOND     (8 bytes)                                             |
       +                                                                                              +
       +--+--+--+--+--+--+--+--+--+--+--+--+--+--+--+--+--+--+--+--+--+--+--+--+--+--+--+--+--+--+--+--+
       | CHANNEL ACCUMULATED PHASE          (8 bytes)                                                  |
       +                                                                                              +
       +--+--+--+--+--+--+--+--+--+--+--+--+--+--+--+--+--+--+--+--+--+--+--+--+--+--+--+--+--+--+--+--+
       | CHANNEL PHASE POLYNOMIAL COEFFICIENT 0      (8 bytes)                                         |
       +                                                                                              +
       +--+--+--+--+--+--+--+--+--+--+--+--+--+--+--+--+--+--+--+--+--+--+--+--+--+--+--+--+--+--+--+--+
       | CHANNEL PHASE POLYNOMIAL COEFFICIENT 1      (8 bytes)                                         |
       +                                                                                              +
       +--+--+--+--+--+--+--+--+--+--+--+--+--+--+--+--+--+--+--+--+--+--+--+--+--+--+--+--+--+--+--+--+
       | CHANNEL PHASE POLYNOMIAL COEFFICIENT 2      (8 bytes)                                         |
       +                                                                                              +
       +--+--+--+--+--+--+--+--+--+--+--+--+--+--+--+--+--+--+--+--+--+--+--+--+--+--+--+--+--+--+--+--+
       | CHANNEL PHASE POLYNOMIAL COEFFICIENT 3      (8 bytes)                                         |
       +                                                                                              +
       +--+--+--+--+--+--+--+--+--+--+--+--+--+--+--+--+--+--+--+--+--+--+--+--+--+--+--+--+--+--+--+--+
       | EMPTY FIELDS FUTURE USE     (36 bytes)                                                        |
       |                                              ...                                             |
       +--+--+--+--+--+--+--+--+--+--+--+--+--+--+--+--+--+--+--+--+--+--+--+--+--+--+--+--+--+--+--+--+
       | EMPTY FIELDS INTERNAL AGENCY USE (40 bytes)                                                   |
       |                                              ...                                             |
       +--+--+--+--+--+--+--+--+--+--+--+--+--+--+--+--+--+--+--+--+--+--+--+--+--+--+--+--+--+--+--+--+
       | END LABEL                                                                                    |
       +--+--+--+--+--+--+--+--+--+--+--+--+--+--+--+--+--+--+--+--+--+--+--+--+--+--+--+--+--+--+--+--+
       |8 |7 |6 |5 |4 |3 |2 |1 |8 |7 |6 |5 |4 |3 |2 |1 |8 |7 |6 |5 |4 |3 |2 |1 |8 |7 |6 |5 |4 |3 |2 |1 |
       +--+--+--+--+--+--+--+--+--+--+--+--+--+--+--+--+--+--+--+--+--+--+--+--+--+--+--+--+--+--+--+--+
```

Figure 10.1: General Structure of Header

is not possible as the registers available in memory is limited. Hence the data needs to be analyzed record by record allowing us to process only 400kB data at a time. This reduces the cost of processing.

The programming language used is IDL (Interactive development Language) which is preferred when it comes to large data analysis. Especially in areas of science, such as astronomy, atmospheric physics and medical imaging as it shares some of its constructs with Fortran and C. Main features are that it provides a simple and efficient index slice syntax to extract smaller chunks of data from large data. Also, it supports few multi-threaded functions improving the efficiency of programming.

10.2. Meta-Data extraction

The metadata present in the RDEF files are extracted initially starting with the observation file. The epoch time for the particular RO session under consideration, along with the transmitted frequency is extracted as mentioned below.

Each line in an observation file starts with a marker. For instance, it uses "#" for comments, V for version number, R for receiver ID, T for transmitter ID, S for scan information (it contains along with other information, the scan number, start of the epoch, end of the epoch, and transmitted frequency), D for the data file information (which includes product file name) for that particular scan number and Z for the end of file.

Hence, the marker is analyzed and will read only the scan line from which the start time and end time are extracted. The number of seconds contained is calculated, which is nothing but the number of records the product file contains.

The transmitted frequency is also extracted from the observation file. Then, each record is extracted sequentially. Before processing the data, the header information is extracted. Mainly, the second of the day (the number of seconds passed in that day before recording that particular Record), sample size (whether the data is 1-bit, 2-bit, 4-bit, 8-bit or 16-bit), sample rate, RF-IF down-conversion factor, and the IF-channel down-conversion factor are extracted. Followed by data extraction

10.3 Pre-Processing

As discussed, the data is packed in a 32-Bit word depending on the sample size and is arranged in an alternating fashion of In-phase component and Quadrature-phase component. Since our data is an 8-bit data, each sample is packed in a word as shown in Figure 9.1. Hence, the data is initially read as an 8-bit data and then converted to 2's complement form. Also, as pointed out earlier, truncation correction is required for this data. Hence, the truncation correction is applied after converting the data to [-1,1] which in the process improves precision

MSB		8-Bit Samples		LSB
Q2	I2	Q1	I1

Figure 10.2: Word packing for a sample of sample size 8

10.4 Flow Chart for Data processing:
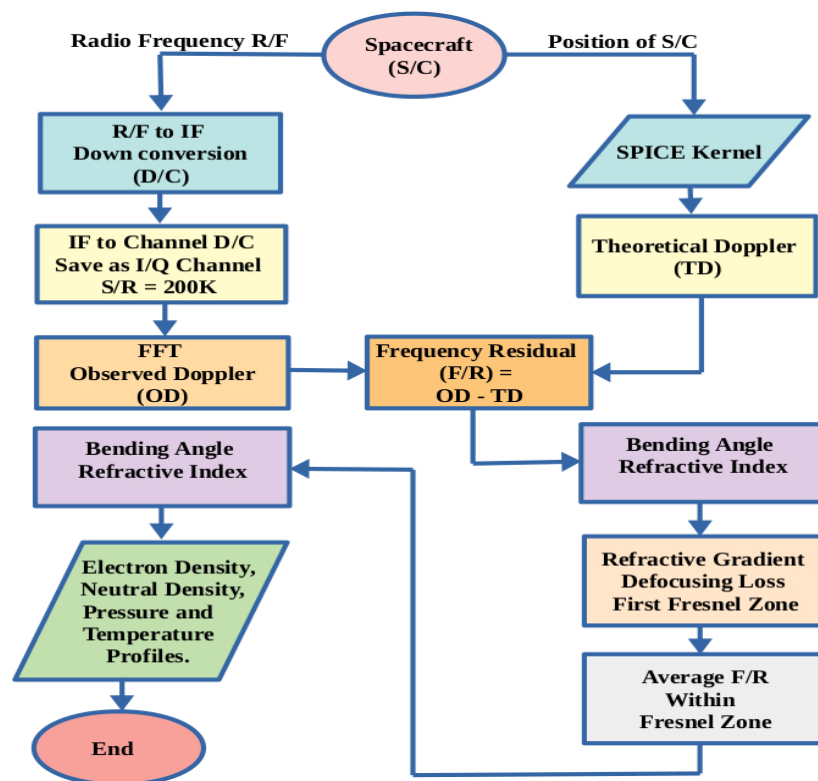
Figure 10.3: Data Analysis Flow Chart

10.4.1 Spacecraft (S/C):

Spacecraft is the location where transmitters are placed to send signals back to Earth. For DFRS aboard CH2, there are two antenna systems onboard which have been deployed for this purpose. The Directional Gain Antenna (DGA) system, which is a parabolic antenna, is used to transmit X-band radio signals, which a S-band patch antenna which have been specially deployed onboard CH2 for transmitting S-band DFRS signals. The transmitter of spacecraft, which is in phase lock with telemetry tracking command signal, generates radio signals after triggered from the ground station. The desirable condition for the spacecraft is to be spin proof, and should have very stable orbit. It should have very narrow beam width for avoiding reflection from surface. In addition to that the desired condition for narrow beam width, the distance of spacecraft should be minimum (since it diverges like r^2).

10.4.2 Radio Frequency(RF):

For probing Lunar atmosphere-ionosphere we selected radio frequencies at X and S bands. The rationale behind selection of these radio signals are the followings

1. It should not be get reflected back from the Ionosphere of Earth as well as the probing ionosphere.

Example: typical electron density of the Earth's ionosphere is of the order of $5*10^{12}$ m^{-3} so plasma frequency for given density would be order of $9*\sqrt{(5*10^{12})} = 2.1 * 10^7$. So the signal of the frequency greater than $2.1 * 10^7$ Hz can only pass through the ionosphere.

2. Attenuation of the signal in medium is inversely proportional to the square of frequency of transmitted signal. To avoid more attenuation, high frequency signals are chosen.

3. And at the same time it should get disperse by the planetary Ionosphere in observable amount, so that our hardware (oscillator) can detect those changes with high accuracy. Due to this limitation we cannot go for very high frequency to avoid attenuation loss.

For example, if we consider transmitted frequency from optical range like $4*10^{14}$ Hz, then attenuation loss may be get reduce by $\sim10^8$ order (from $\sim 10^{10}$ Hz radio signal) and dispersion of signal will also reduce by same order. So for this case to study the Lunar Ionosphere the stability of clock should be more than 10^{-22} ($\sim1/10^{14}*10^8$) second, which is quite impossible for existing technology.

4. There are small size of particles or clouds presented in the lower neutral atmosphere. These particles can scatter the light in optical/micrometer range as according to their size. There is

also, different species presented in atmosphere whose absorption band lies in higher frequency range. So Signal should not get absorbed/scatter by neutral atmosphere. This also prohibits the option of higher frequency range.

5. The radio signal and their stability, used by different planetary mission is shown in the Figure 9.3.

Table 1. Planetary missions with radio occultation (RO) experiment onboard. The stability is for the radio signals used in the experiment

Spacecraft	Planetary body	Single/dual frequency	Frequency	Stability
Mariner 4	Mars	Single	S 2.3 GHz	$\sim10^{-11}$
Mariner 5	Venus	Dual Beacon	49.8 and 423.3 MHz	$\sim10^{-10}$
		Single	S 2.3 GHz	
Mariner 6	Mars	Single	S 2.3 GHz	$\sim10^{-11}$
Mariner 7	Mars	Single	S 2.3 GHz	$\sim10^{-11}$
Mariner 9	Mars	Single	S 2.3 GHz	$\sim10^{-11}$
Mariner 10	Mercury	Dual	S 2.3 GHz	$\sim10^{-11}$
			X 8.4 GHz	
Voyager 1	Saturn	Dual	S 2.3 GHz	$\sim10^{-12}$
	Jupiter		X 8.4 GHz	
MGS	Mars	Single	X 8.4 GHz	$\sim10^{-13}$
Mars Express	Mars	Dual	S 2.3 GHz	$\sim10^{-14}$
			X 8.4 GHz	
Venus Express	Venus	Dual	S 2.3 GHz	$\sim10^{-13}$
			X 8.4 GHz	
Akatsuki	Venus	Single	X 8.4 GHz	$\sim10^{-12}$
Galileo	Jupiter, Io	Single	S 2.295 GHz	$\sim10^{-12}$
Pioneer 10	Jupiter	Single	S 2.3 GHz	$\sim10^{-10}$
Pioneer 11	Jupiter	Single	S 2.3 GHz	$\sim10^{-10}$
Cassini	Saturn	Three	Ka 32.0 GHz	$\sim10^{-13}$
			X 8.4 GHz	
			S 2.3 GHz	
Voyager 2	Uranus	Dual	S 2.3 GHz	$\sim10^{-12}$
			X 8.4 GHz	
SELENE	Moon	Dual	S 2.3 GHz	$\sim10^{-11}$
			X 8.4 GHz	
New Horizon	Pluto	Dual	S 2.3 GHz	$\sim10^{-13}$
			X 8.4 GHz	

Table 10.1: A table showing frequencies used in different planetary missions (After Choudhary et al 2019)

10.4.3 RF to IF down conversion:

As we can see that in Figure 9.3, transmitted radio signal frequencies in RO experiments are mostly of the order of GHz (10^9). Handling of such a high frequency signals obviously is quite difficult, in terms of power and memory. So without altering the actual information, signal is down converted up to 70MHz (standard, it may be down converted in different frequency as well according to the needs). In open loop receiver mode down conversion frequency could be the same as the transmitted frequency or transmitted frequency plus half of range rate Doppler. It depends on our choice.
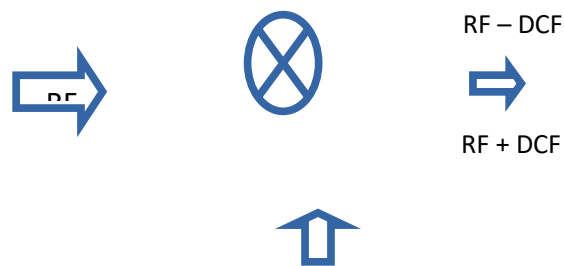
Figure 10.4. Down-conversion frequency (DCF)

Let's take sinusoidal signal of frequency w_1 and frequency of local oscillator as w_2 then at the mixture they interact as

$$y = a_1a_2*\sin(w_1t)*\sin(w_2t)$$

$$= a_1a_2/2 *[2*\sin(w_1t)*\sin(w_2t)]$$

$$= A [\cos(w_1-w_2) -\cos(w_1 + w_2)]$$

where $A = a_1a_2/2$

From the equation 4, the mixture generates two frequency as (w_1-w_2) and frequency $(w_1 + w_2)$ as an output. By applying Low Pass Filter, we can get the expected down-converted frequency.

10.4.4 Sampling: We receive voltage V_o on the ground station and the time series of voltage is recorded in two component, namely in-phase (I, $V_o\cos\theta$) and in-quadrature (Q, $V_o \sin\theta$). All the channel is recorded at a sampling rate of 200000 sample rate.

10.4.5 Fast Fourier Transform (FFT): FFT enables us to change the signal in frequency domain which is recorded in time domain. We have taken I and Q channel and make it complex (original signal) then perform FFT to get the Doppler. The FFT is an advanced version of Discrete Fourier Transform (DFT). Discrete Fourier transform can be computed in (Nlog$_2$N) operations, an algorithm which is called the fast Fourier transform, or FFT (Lipa and Tyler, 1979).

If we have time series function F(t) then Discrete Fourier Transform of the signal could be given by

$$F(k) = \sum_{n=0}^{N-1} F(n)\exp(-j\frac{2\pi}{N}n.k), k = 0,1,.....N-1$$

the Fourier transform of observe signal for one second is shown in Figure 9.4 and corresponding power plot shown in Figure 9.5.

Further if we zoom the Figure 10.6 about the peak power (as shown in Figure 10.7), the spectrum is not perfect Gaussian and it has a finite Doppler width. This width may lead to huge uncertainty in observed Doppler. The reason behind such Doppler width is due to high variation in the relative velocity of the observer and receiver during the sampling period of 1 sec.
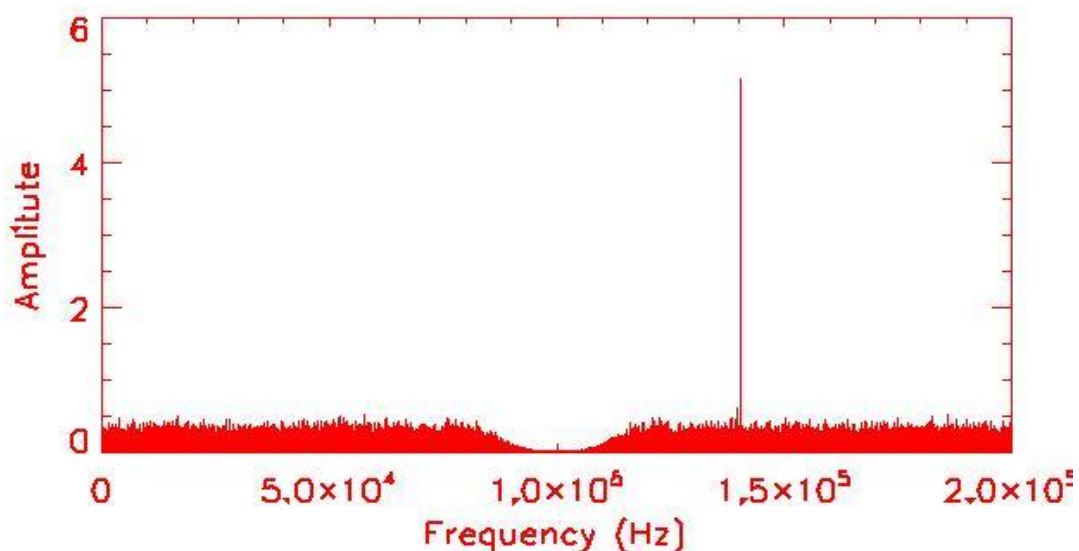
Figure 10.5. FFT for one second complex data.

Frequncy Spectrum for One Sec Data
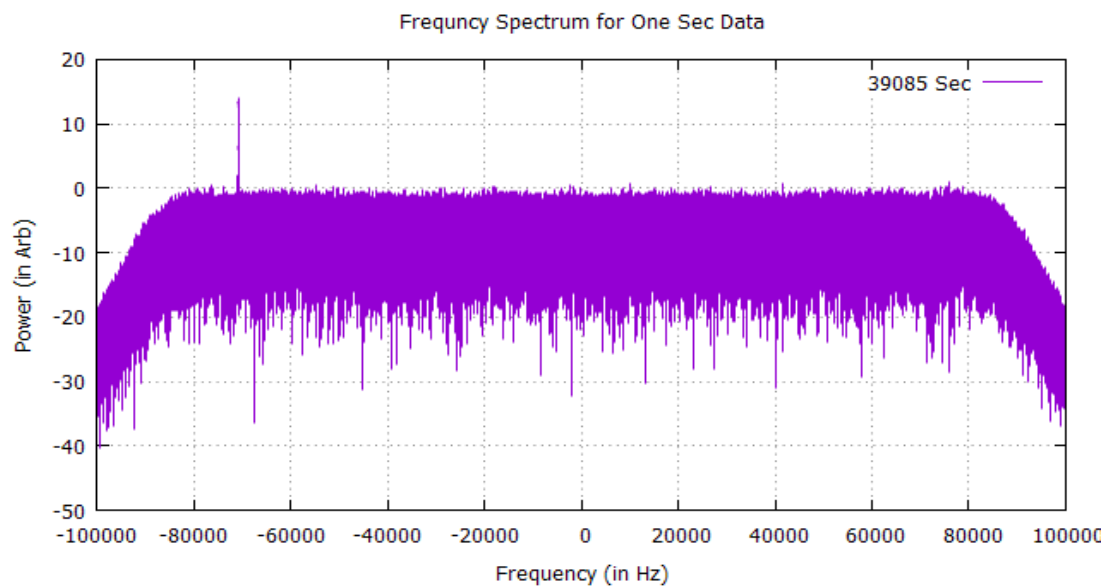
Figure 10.6: Power Spectrum for one sec of open-loop data recorded in RDEF format

Frequncy Spectrum for One Sec Data (Zoomed in on Peak)
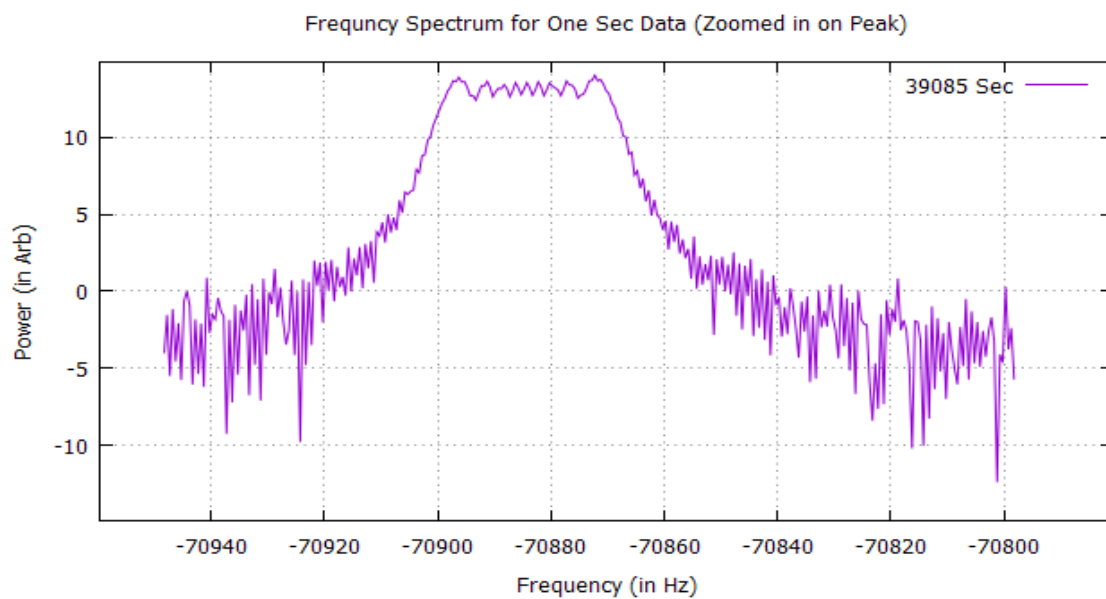
Figure 10.7: Zoomed part of rectangular box of Figure 9.5
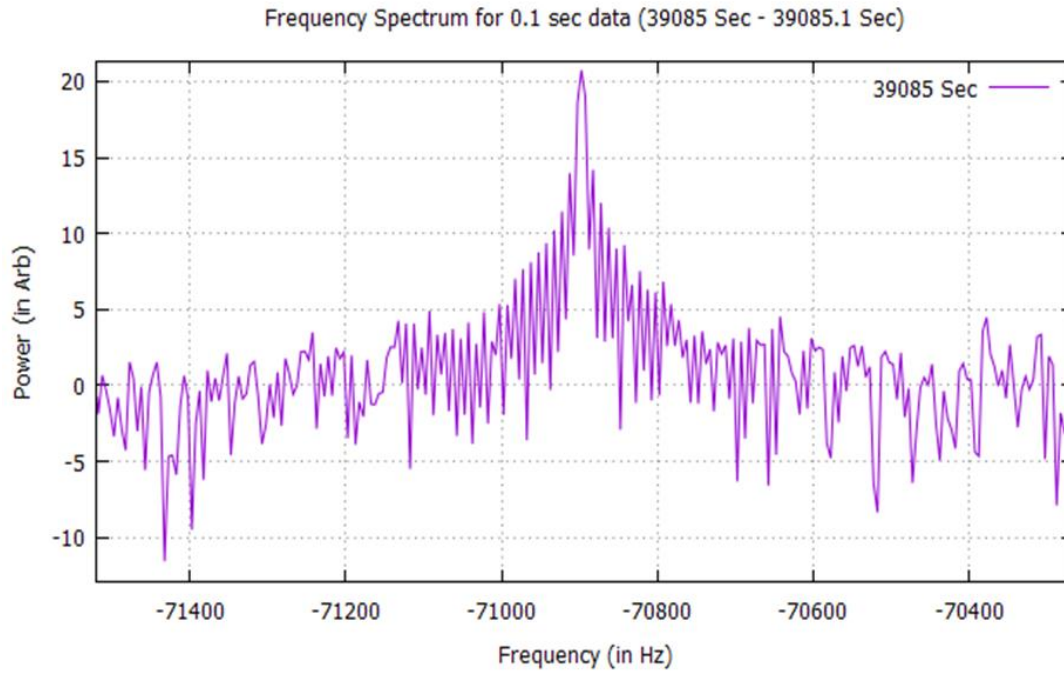
Figure 10.8. For 0.1 second Data. Frequency vs power plot.

To get very precise value of observed Doppler or constant value of relative velocity we tried to improve time resolution and divided signal into 0.1 second (Imamura et al 2017). To achieve higher precision (sample rate / data point taken) in frequency range we padded more zeroes to data in time domain. Then observed frequency and power spectrum shown in Figure 10.8, its almost Gaussian in shape. Applied the quadrature fit and then calculated Zeroth moments and first moments for estimating total observed power and Doppler. Detailed description on various steps involved with the data processing is given in appendixes.

To calculate the moments we took 128 data point around observed peak power in Figure 10.8 and followed the method by Woodman et al 1985.

$Zeroth momtnts, p = \sum_{i=1}^{N} S(w_i)$

where $S(w_i)$ is power spectrum function , w is the frequency and N is the number of data point taken

$First moments, \Omega = \frac{1}{p} \sum_{i=1}^{N} w_i S(w_i)$

Here P and Ω are total signal power and observed Doppler respectively.

10.5 Observed Doppler:

Transmitted radio signals suffer changes in frequency (Doppler) due to relative velocity of the observer and receiver, effect of planetary gravity, interplanetary medium, terrestrial atmosphere and of course the effect of the atmosphere of targeted planetary body. To calculate total observed power, we followed equation 6. The Doppler is the first moments of the Gaussian curve estimated using equation 7.

For estimating actual Doppler shift which occurs in the observed radio signals, we added Doppler obtain after FFT with the down conversion frequency and subtracted with transmitted frequency.

Observed Doppler = Down conversion Frequency + FFT value (Doppler) – Transmitted frequency

10.6 Theoretical Doppler/Range-rate Doppler:

Christian Doppler was the first person who proposed in 1842 that the received signal suffers changes in frequency due to the relative motion between transmitter and receiver. Received frequency exceeds the transmitted frequency value if receiver and observer are approaching each other and vice versa. The general non relativistic formula for change in frequency was given as

$f = f_0[(c + v_r)/(c + v_s)]$

where, f – observed frequency

f_0 – transmitted frequency

c – speed of wave in medium

v_s – velocity of source, positive if approaching toward the observer and negative if it's going away from the observer

v_r – Velocity of the observer, negative if approaching toward the source and positive if it's going away from the source.

From the Einstein Equivalent principle (EEP), 'there is numerical equality between the inertial and gravitational mass that the acceleration is independent of the nature of the body'. When an electromagnetic wave passes through the planetary body it suffers bending due to the

gravitational force, velocity of signal toward the observer get modified, hence suffer the change in their frequency.

We followed the Krisher's approach (Krisher et al 1993) to compute total Doppler change suffer by the transmitted radio signal as:

$$F_2 = F_1 [1- \mathbf{n}.(\mathbf{v}_1-\mathbf{v}_2)/c - (v_1^2-v_2^2)/c^2 - (\mathbf{n}.\mathbf{v}_1)(\mathbf{n}.\mathbf{v}_2)/c^2 + (\mathbf{n}.\mathbf{v}_1)^2/c^2 - (U_1 - U_2)/c^2]$$

Where $\mathbf{n}$ is the unit vector along the line joining to the transmitter and receiver and 'c' is the speed of light. V_1 is the velocity of the transmitter and V_2 is the velocity of receiver, U_1 and U_2 are the total Newtonian gravitational potentials at both point respectively. F_1 and F_2 are the transmitted and received signal frequencies.

10.7 Effect of atmosphere over Signal:

Radio signals bend toward the planetary body while passing through the neutral atmosphere of that planet. The refractive index of neutral medium is always greater than 1, in equation 1, (1-a) will be the negative value which implies that the signal will suffer phase loss while passing through the neutral atmosphere. This phase change reflects change in the Doppler. The effect of atmosphere over signal may be obtained by removing range-rate/theoretical Doppler from total observed Doppler.

Atmospheric Doppler = Observed Doppler – Theoretical Doppler

10.8 Frequency Residual(Δf):

The bending of radio signals, and hence phase loss occurs when radio signals pass through the neutral medium. On the other hand, dispersion of the radio signals, which is dependent on the frequency, results in phase gain for the signals. The phase loss and gain is inherent in the received radio signals and deciphered from the frequency residuals which is nothing but the difference in the observed and predicted Doppler frequencies of the probing radio signals. Our primary objective in RO experiments therefore is to obtain the change in phase/Doppler (Δf = dϕ/dt where f, ϕ, t are frequency , phase and time respectively) due to atmosphere of targeted planetary object. To know the effect of interplanetary medium and terrestrial atmosphere we conduct experiments prior to 10 minutes before signal passing through the planetary atmosphere. The sampled data during this period is used as a baseline and extrapolated up to the complete experiments and remove that effect from the complete data set. The assumption here is that there is no abrupt change in terrestrial/interplanetary

medium during atmospheric occultation time (~ 2 minute). The remaining part of Doppler will be the effect of planetary atmosphere only.

10.9 Impact parameter:

It is defined as a closest approach of radio signal toward target planet in absence of planetary atmosphere. It is challenging to compute the point of closest approach, since all the body like, spacecraft, target and observer are moving in different plane. We selected J2000 frame as Cartesian coordinate system and choose the position of origin at planetary barycenter. SPICE kernel was used to determine the position and velocity of these bodies in given time of reference. But still these bodies were not in the same plane.

Next challenge was to bring all of them in same plane, the plane which may contain the trajectory of radio waves, position of spacecraft, position of target body and the position of receiver (Fjeldbo et al 1971). Let us then define a new co-ordinate system in such a way that, the line joining to the receiver and center of target planet is the Z axis, normalized for the unit vector ($\hat{z}$), as the position of receiver is obtained at the time when radio signal reaches toward the receiver end (time at target + time of light needed to reach the receiver). Obtain the position of spacecraft with respect to the center of target body, take the cross product between the position vectors, receiver to target planet and target planet to spacecraft and normalized it, which will give the unit vector ($\hat{n}$) and again take cross product of ($\hat{n}$) and ($\hat{z}$) will give the unit vector ($\hat{r}$) , as shown in Figure 10.9.

Consider the position of the spacecraft 'S' at time t_s , position of receiver 'T' at time t_t and position of target 'O' at time t_0 in J2000 frame of reference, from the point of solar system barycenter (SSB) the unit vector of new coordinate system may be defined as

$$\hat{z} = \frac{[\bar{O}(t_o) - \bar{T}(t_t)]}{|[\bar{O}(t_o) - \bar{T}(t_t)]|} \qquad \hat{n} = \frac{[\bar{S}(t_s) - \bar{O}(t_o)]}{|[\bar{S}(t_s) - \bar{O}(t_o)]|} \times \hat{z} \qquad \hat{r} = \hat{z} \times \hat{n}$$
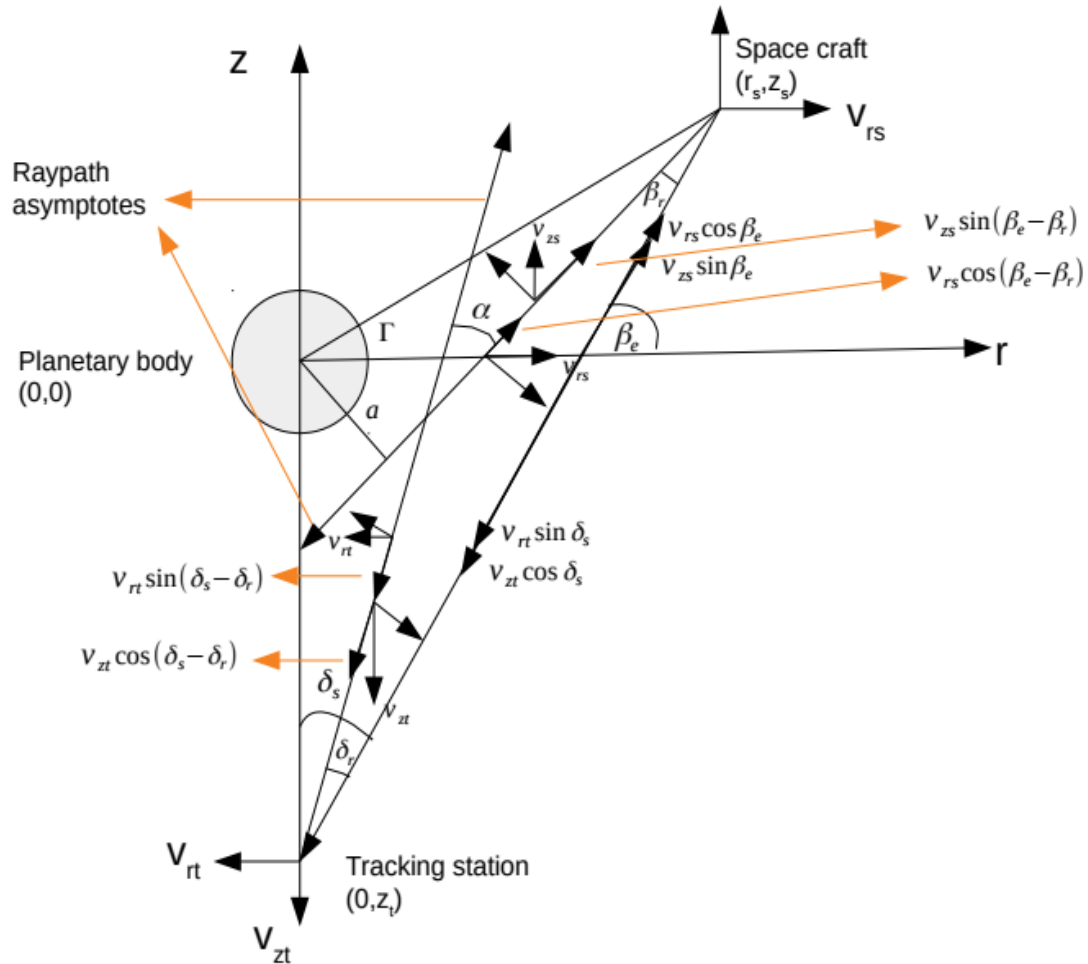
Figure 10.9: *Ray digram of typical Radio Occultation (RO) experiments. Where α is bending angle, v_{zs}, v_{rs} is component of the velocity of spacecraft in z and r direction respectivelly, similarly v_{zt}, v_{rt} is the component of the velocity of ground station is z and r direction respectivelly.*

now we can resolve the position and velocity of spacecraft, target body and receiver in our newly formed co-ordinate system. So from the figure impact parameter 'a' can be calculated as

$$a = (\sqrt{r_s^2(t_s) + z_s^2(t_s)}) \times \sin(\beta_e - \beta_r - \gamma) = -Z_t(t_t)\sin(\delta_s - \delta_r)$$

where a – impact parameter

rs, zs is the position component of the spacecraft and similarly Zt is the zth component of the position of receiver.

βe – Angle between line joining the spacecraft and receiver with rth axis of co-ordinate system.

βr - Angle between lines, joining spacecraft to impact point (in presence of atmosphere) and spacecraft to receiver end.

Gama – angle between r axis and line joining target center to spacecraft

δr - angle between the traces of radio signal (in presence of atmosphere and in absence of atmosphere)

δs – angle between line joining receiver to spacecraft and receiver to center of target body.

10.10 Bending Angle:

In geometrical optics the direction of propagation of the ray is determined by the gradient of the refractive index (Born and Wolf, 1959).

$$\frac{d}{dr}(n\hat{r}) = \bar{\nabla}n$$

here n is refractive index, r is the unit vector along the direction of propagation.

Depending upon the variations in the refractive index, the radio signal suffers bending in the medium. This bending can be estimated from the above geometry, as shown in the Figure 9.10. If we retrace the path of the signal when it was entering the medium and while it was leaving the medium, the asymptotes of the signal will intersect at a point and give the net bending angle of the signal. Measurements of bending angle thus provide all the basic information about atmosphere. From the figure 13 the bending angle could be

$$\alpha = \delta_r + \beta_r$$

Where δ_r and β_r is shown in Figure 9.10

Following the classical mechanical approach, the change in frequency (Doppler) could be estimated as

$$\Delta f = \frac{-v_{ts}}{c} \times f$$

where v_{ts} = velocity of source – velocity of receiver

  f = transmitted frequency

  c = speed of light

if we resolve the component of velocities in the direction of actual path and along the straight line path (in absence of atmosphere) as shown in figure. Doppler along the straight line path (in absence of Atmosphere) is

$$\Delta f_N = \frac{f_s}{c}[c + v_{rt}\sin(\delta_s) + v_{zt}\cos(\delta_s) - v_{rs}\cos(\beta_e) - v_{zs}\sin(\beta_e)]$$

where f_s is the transmitted frequency of the signal and other terms is shown in figure 13.

Now include the atmosphere as well then the change in observed Doppler could be

$$\Delta f_A = \frac{f_s}{c}[c + v_{rt}\sin(\delta_s - \delta_r) + v_{zt}\cos(\delta_s - \delta_r) - v_{rs}\cos(\beta_e - \beta_r) - v_{zs}\sin(\beta_e - \beta_r)]$$

so frequency residual could be

$$\Delta f = \Delta f_A - \Delta f_N$$

$$\Delta f = \frac{f_s}{c}[v_{rt}(\sin(\delta_s - \delta_r) - \sin(\delta_s)) + v_{zt}(\cos(\delta_s - \delta_r) - \cos(\delta_s)) - v_{rs}(\cos(\beta_e - \beta_r) - \cos(\beta_e)) - v_{zs}(\sin(\beta_e - \beta_r) - \sin(\beta_e))]$$

Here δ_s and β_e can be estimated on the basis of geometry (Figure 9.10), Δf is known (observed). I n equation '11', value of angle gamma could also be estimated from geometry. So two equation and two unknown (δ_r and β_r), could be easily calculated. Now bending angle would be

$$\alpha = \delta_r + \beta_r$$

To get the variation in the bending angle with altitude, we have to approximate atmosphere as spherically symmetric and divide them in several homogeneous spherical shell, like the layers of onion. That is why, it is also known as onion peeling technique.

10.11 Refractive index:

Bending of the radio signal is depends upon variation in the refractive index of the medium. To obtain the vertical profile of refractive index we have to follow the Abel transformation (Fjeldbo et al 1971).

$$\mu(a_1) = \exp[\frac{1}{\pi} \int_{\alpha(a_1)}^{\alpha=0} \ln(\frac{a(\alpha)}{a_1} - [(\frac{a(\alpha)}{a_1})^2 - 1]^{1/2}) \, d\alpha]$$

Where a is impact parameter and μ is the refractive index of the medium.

10.12 Number Density:

Refractive index is the property of the medium, it is depending upon concentration of particle and their nature. Atmosphere mainly consists of two type of medium, Neutral medium and charged medium. An electromagnetic wave suffer dispersion when it passes through the charged medium. Which depending upon refractive index of the medium. For planetary Ionosphere $\mu_e - 1 = v_e n_e$, where n_e is the concentration of electron in medium and v_e is the refractive volume of electron (Eshleman et al 1973). The refractive volume of electron may depend upon size of electron in one dimension and wavelength of signal in another two dimension (Eshleman et al 1973). So

$$v_e = r_e \lambda^2/2\pi$$

where $r_e = 2.85 * 10^{-15}$ is the radius of electron and λ is the wavelength

putting all values together we will get

$$\mu_e - 1 = \frac{-40.3 n_e}{f^2}$$

where f is the frequency of the signal.

With the help of equation 19, vertical profile of refractive index is already estimated. By utilizing equation 20 the vertical profile of planetary ionosphere could be estimated.

When signal passes through the neutral atmosphere it suffer refraction, which depend upon the refractive index of the medium. For molecular atmosphere refractivity, $\mu_n - 1 = v_n n_n$, where n_n is the neutral density of the atmosphere and v_n is the average refractive volume of the presented molecules in the medium.

$$v_n = \sum_i \frac{v_i n_i}{n_n}$$

where v_i is the refractive volume of the ith molecules whose concentration is n_i.

Values of v_i and v_n, in pure non-polar gases and their mixtures appear to be independent of concentration, temperature, or pressure over wide ranges of these variables (see for example Tyler and Howard 1969). In the case of polar molecules like H_2O, this may inversely depend over temperature.

Range of refractive volume is varies between 0.5 to 5 * 10^{-29} m^3 , which is approximately equivalent to the geometrical volume of the molecules (Eshelman et al 1973). Therefore, refractivity profile of neutral, molecular and non-polar atmosphere could be

$\mu_n -1 = v_n n_n$

10.13 Retrieval of Temperature profile:

It is very good approximation to consider hydro-static equilibrium condition for well mixed planetary atmosphere, we can derive temperature profile from (Silvia Tellman et al 2009)

$$T(h) = \frac{\mu_{up}}{\mu} T_{up} + \frac{m}{n(h).k} \int_h^{h_{up}} n(h')g(h')dh'$$

where 'up' stand for the upper boundary condition for detectable atmosphere.

Using the Ideal gas equation

$P(h) = n(h).K.T(h)$

Pressure profile of the Neutral atmosphere is also computed.

Vertical resolution: Vertical resolution is one important factor while trying to determine the atmospheric/ionospheric profile. The vertical resolution during occultation experiments is limited by the diameter of the first Fresnel zone. However, the refraction in the atmosphere changes the Fresnel zone shape from circular to elliptical form, and the resulting vertical diameter becomes (Fjeldbo and Eshleman, 1969; Karayel and Hinson, 1997)

$$d_v = 2\sqrt{\lambda DL},$$

where λ is the wave-length of the carrier signal (i.e. 3.6cm for X-band and 13.03cm for S-band).

10.14 Sources of error:

10.14.1 Atmospheric defocusing and absorption:
The received signal power during each occultation experiment varies due to atmospheric defocusing and absorption, which must be taken into account while retrieving the vertical distribution of atmospheric/ ionospheric constituents that may contribute to absorption of the signal power.

Atmospheric defocusing is caused by the radial gradient of the refractive index, and the defocusing loss is estimated as (Eshleman, 1973)

$$L = (\cos\alpha - D\frac{d\alpha}{da})^{-1},$$

where D is the distance from the spacecraft to the crossing of the ray-asymptotes. The loss increases with the value of D. Each of D, α and a varies as the S/C moves in its trajectory, and from that information, the defocussing loss can be estimated as a function of time, which in turn can be converted to the height profile of the absorptivity of the atmosphere/ionosphere.

10.14.2 Thermal noise of the radio receiver: The major noise source responsible for the Doppler velocity measurement error is the thermal noise of the radio receiver at the G/S. The velocity error σ_v contributed by the ground station is given as

$$\sigma_v = \frac{c}{4\pi f \Delta t}\sqrt{\frac{2BN_0}{C}},$$

Where B is the receiver bandwidth, C and N_0 are receiver carrier-power and noise-power densities respectively. Another source contributing to the velocity error is the transponder phase noise σ_φ:

$$\sigma_v = \frac{c\sqrt{2}}{4\pi f t}\sigma_\varphi.$$

The transponder phase noise σ_φ has to be determined experimentally, as has been done by Remus et. al (2001).

10.14.3 Light-time corrections: During interplanetary missions, the travel time of the radio-wave from the S/C to the G/S cannot be neglected - the occultation at Moon would take place at an earlier time than it would be observed at the G/S. Due to the finite velocity of light, the geometric relative positions of S/C, Moon, and G/S at time of signal reception are different from those at the time of signal emission. The value of the light-time correction depends on the relative position of the celestial body and Earth, at any instant of time, however it must be included in the analysis.

10.14.4 Tropospheric Refraction of Earth's Atmosphere: Before reaching the G/S on Earth, the radio-signal would travel through Earth's atmosphere as well, and the effect of the neutral atmosphere is denoted as tropospheric refraction. The neutral atmosphere is a non-dispersive

medium at radio-frequencies up to 15 GHz, however, the refractive index n is dependent on air pressure, temperature, humidity and zenith angle.

The tropospheric contribution to the refractivity μ of the neutral atmospheric of Earth can be expressed as a summation of two terms: the dry component μ_{dry} because of the dry air and the wet component μ_{wet} because of the water vapour present in the atmosphere. The complete expression for the tropospheric refractivity is given by the empirical formula:

$$\mu_{Tropo} = 77.624\frac{p}{T} + 371900\frac{e}{T^2} - 12.92\frac{e}{T},$$

where p is the atmosphere pressure in hPa, e is the atmospheric vapour pressure in hPa and T is the surface-temperature in Kelvin. The dry atmosphere contributes almost 90% of the total tropospheric refractivity.

Change in the bending angle in the Earth's atmosphere, $\Delta\alpha$, can be estimated as

$$\Delta\alpha = \mu.10^{-6}.\frac{1}{\tan\theta},$$

where θ is equivalent to the elevation angle of the G/S antenna given in radian.

11. References:

1. Baum, W.A. and Code, A.D., 1953. A photometric observation of the occultation of Sigma Arietis by Jupiter. The Astronomical Journal, 58, pp.108-112.

2. Born, M. and Wolf, E., 1959. Principles of optics, 1964. New York: Mac-Millan.

3. Choudhary, R.K., Bindu, K.R., Harshit, K., Karkara, R., Ambili, K.M., Pant, T.K., Shenoy, D., Kumar, C., Reddy, N., Rajendran, T.K. and Nazer, M., 2020. Dual Frequency Radio Science experiment onboard Chandrayaan-2: a radio occultation technique to study temporal and spatial variations in the surface-bound ionosphere of the Moon. Current Science (00113891), 118(2).

4. Elliot, J.L., 1979. Stellar occultation studies of the solar system. Annual review of Astronomy and Astrophysics, 17(1), pp.445-475.

5. Esposito, L.W., O'callaghan, M. and West, R.A., 1983. The structure of Saturn's rings: Implications from the Voyager stellar occultation. Icarus, 56(3), pp.439-452.

6. Eshleman, V.R., 1973. The radio occultation method for the study of planetary atmospheres. Planetary And Space Science, 21(9), pp.1521-1531.

7. Fjeldbo, G., Kliore, A.J. and Eshleman, V.R., 1971. The neutral atmosphere of Venus as studied with the Mariner V radio occultation experiments. The Astronomical Journal, 76, p.123.

8. Imamura, T., Ando, H., Tellmann, S., Pätzold, M., Häusler, B., Yamazaki, A., Sato, T.M., Noguchi, K., Futaana, Y., Oschlisniok, J. and Limaye, S., 2017. Initial performance of the radio occultation experiment in the Venus orbiter mission Akatsuki. Earth, Planets and Space, 69(1), pp.1-11.

9. Krisher, T.P., 1993. Parametrized post-Newtonian gravitational redshift. Physical Review D, 48(10), p.4639.

10. Lipa, B. and Tyler, G.L., 1979. Statistical and computational uncertainties in atmospheric profiles from radio occultation: Mariner 10 at Venus. Icarus, 39(2), pp.192-208.

11. Pätzold, M., Häusler, B., Tyler, G.L., Andert, T., Asmar, S.W., Bird, M.K., Dehant, V., Hinson, D.P., Rosenblatt, P., Simpson, R.A. and Tellmann, S., 2016. Mars express 10 years at mars: observations by the Mars express radio science experiment (MaRS). Planetary and Space Science, 127, pp.44-90.

12. Tellmann, S., Pätzold, M., Häusler, B., Bird, M.K. and Tyler, G.L., 2009. Structure of the Venus neutral atmosphere as observed by the Radio Science experiment VeRa on Venus Express. Journal of Geophysical Research: Planets, 114(E9).

13. Woodman, R.F., 1985. Spectral moment estimation in MST radars. Radio Science, 20(6), pp.1185-1195.

Appendix 1: Fourier Transform

The graphical representation of the time domain and frequency domain is shown in Figure A1-1.
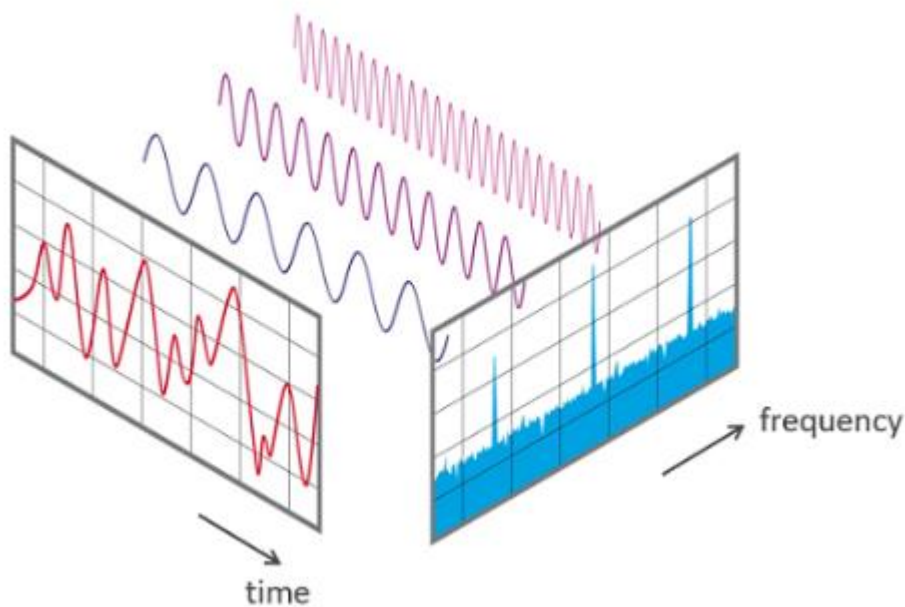
Figure A1-1: Representation of Frequency Domain and Time Domain Concept

Fourier Transform works due to the fact that each and every signal can be modeled as the linear combination of sines and also the fact that when 2 sine-waves are multiplied, the average of the resulting signal is proportional to the amplitude of the sine-wave if they are of same frequency and is 0 if they differ in frequency. If there is a phase difference, then the amplitude will be proportional to the cosine of the difference of the phases.

Fast Fourier transform (FFT) is an algorithm that computes the Discrete Fourier Transform (DFT) by exploiting the property of symmetry in DFT. Fourier Transform is given by

$$X_k = \sum_{n=0}^{N-1} x_n . e^{-i2\pi k \frac{n}{N}}$$

where x_n is the data sample, $e^{\frac{-2\pi ikn}{N}}$ is the eigen vector or basis of the transformation. N is the number of Fourier Transform points taken. Here the number of computation is N^2.

The Inverse Fourier Transform is identical to the Fourier Transform except for scaling.

$$x_n = \frac{1}{N}\sum_{n=0}^{N-1} X_k . e^{i2\pi k \frac{n}{N}}$$

where x_n is the reconstructed data sample, X_k is the frequency component, $e^{\frac{2\pi ikn}{N}}$ is the eigen-vector or basis of the transformation. N is the number of FFT points.

A1.1. Fast Fourier Transform in the West (FFTW)

The FFTW is known to be the fastest free software implementation of FFT. What FFTW does is that instead of holding onto a single algorithm for FFT, it supports a variety of algorithms hence enabling it to choose the optimum algorithm depending on the data structure. Initially, it will analyze the data whose FFT has to be determined, and FFT is calculated using the algorithm it determines to be optimized for that particular data set. It works best with small prime factors, with powers of 2 being optimum.

For a one-dimensional FFT, the cost of computation is proportional to the total number of points in data times a linear function of the times for its prime factors.

If N is the total data length, then

$$N = 2^{K_2} 3^{K_3} 4^{K_4} \dots$$

The time taken is

$$T_f = T_0 + N(T_1 + 2T_2 K_2 + T_3(3K_3 + 5K_5 + \dots))$$

Also, it is to be noted that $T_3 4 T_2$.

The C subroutine for FFTW is available for free at www.fftw.org. Also, programming languages like MATLAB and IDL use FFTW. It is customizable in MATLAB. These programming languages support multi-threading allowing faster computations.

A couple of FFT algorithms will be discussed in the following sections.

A1.2. Prime-factor FFT algorithm

Here, the data is expressed as a composite set of prime numbers (i.e. $N = N_1 N_2$, where N_1 and N_2 are relatively prime) and then dividing it into smaller transformations of the size N_1 and N_2, where these transformations are calculated by re-indexing the input and output series successively which on substitution creates a nested DFT transformation.

Re-indexing the input

$$N = n_1 N_1 + n_2 N_2$$

$$k = k_1 N_1^{-1} N_1 + k_2 N_2^{-1} N_2$$

where N_1^{-1} and N_2^{-1} are the multiplicative inverse of N_1 modulo N_2 and the multiplicative inverse of N_2 modulo N_1 respectively, k_i and n_i vary from 0, 1, ..., $N_i - 1$ which is nothing but a solution to the Chinese Remainder Theorem (CRT). The resultant nested DFT is given by

$$X_{k_1 N_2^{-1} N_2 + k_2 N_1^{-1} N_1} = \sum_{n_1=0}^{N_1-1} \left(\sum_{n_2=0}^{N_2-1} x_{n_1 N_2 + n_2 N_1} e^{-\frac{2\pi i}{N_2} n_2 k_2} \right) e^{-\frac{2\pi i}{N_1} n_1 k_1}$$

A1.3 Cooley-Tukey Algorithm

Cooley-Tukey Algorithm is the most widely used algorithm. Here the number of data is expressed as a composite set (i.e. $N = N_1 N_2$), thus dividing it into smaller transformations of size N_1 and N_2. Radix-2 Decimation is the simplest and the most common implementation of this algorithm.

$$X_k = \sum_{m=0}^{N/2-1} x_{2m} e^{-i2\pi k \frac{2m}{N}} + \sum_{m=0}^{N/2-1} x_{2m+1} e^{-i2\pi k \frac{2m+1}{N}}$$

$$= \sum_{m=0}^{N/2-1} x_{2m} e^{-i2\pi k \frac{m}{N/2}} + e^{-i2\pi \frac{k}{N}} \sum_{m=0}^{N/2-1} x_{2m+1} e^{-i2\pi k \frac{m}{N/2}}$$

where m =0,1,2, …
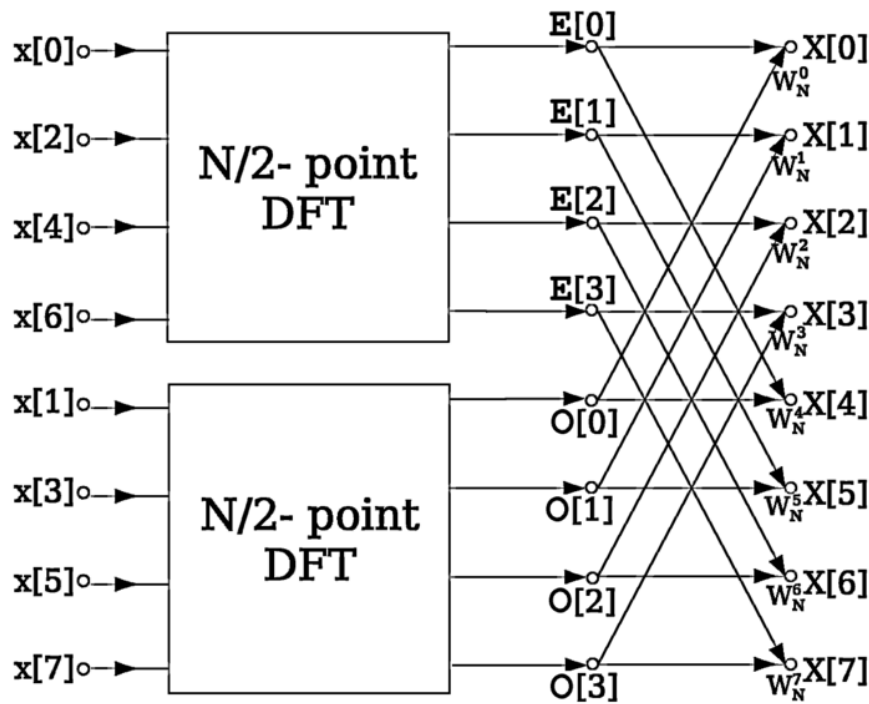
Figure A1-2 : Radix-2 Decimation in Time

On dividing the data into odd and even parts we can see that they are similar to each other except for multiplication of complex root of unity which is called the twiddle factor. Hence, it is sufficient to calculate only one set (even or odd), and thus reducing the computational

complexity to $\frac{N^2}{2}$. If we are able to divide it further, the calculations reduce to complexity to $O(N\log(N)))$.

In short, FFT is the fastest implementation of Fourier transform as it reduces the computation complexity from $O(N^2))$. to $O(N\log(N)))$. by removing redundant calculations.

Hence, using data of length as a power of 2, this algorithm can be optimized. Without altering the signal spectrum, the length can be increased by padding desired number of zeros. But care must be taken in order to maintain the cost of computation. As the number of data points increases, computation time increases.

Resolution is defined as the ratio between the sampling rate and the number of FFT points taken (i.e. $Res = f_{s1}/n_{fft}$). As FFT points increase, resolution value reduces thus improving resolution. As can be seen in Figure A1-3, as resolution value decreases (improved resolution), time taken increases exponentially.
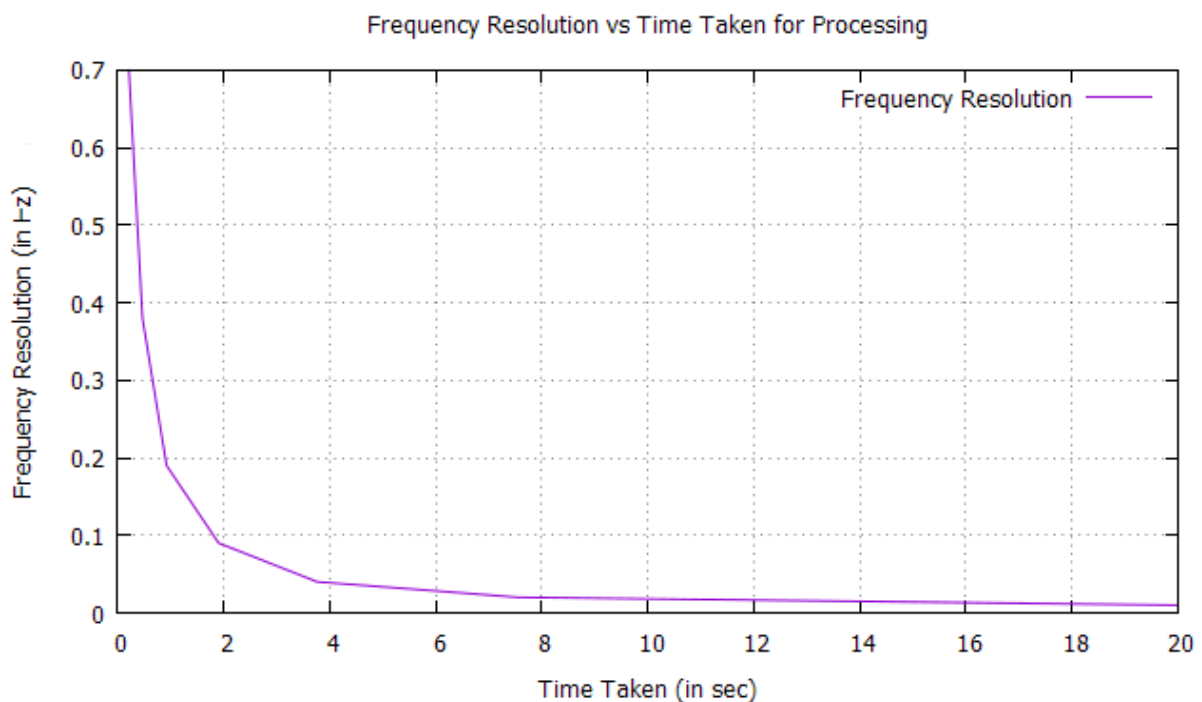
Figure A1-3: Resolution VS Time Taken for computation of FFT

A1.4. Other Algorithms

Some of the other algorithms include:

1. Bruun's Algorithm uses successive polynomial factorization. Since it used real coefficients until the last stage, it did not get enough momentum for widespread usage.

2. Rader's Algorithm uses successive cyclic convolution of DFT of prime numbers. But can be used only for lower order transform.

3. Hexagonal Fast Fourier Transform computes FFT for the hexagonally sampled data using addressing scheme for hexagonal grids known as Array Set Addressing (ASA).

A1.5. FFT in RO

In this study, the main requirement is to extract the Doppler shift from the data received. For this, the data is transformed from the time domain to the frequency domain using Fast Fourier transform. IDL uses FFTW and since the Cooley-Tukey algorithm is the most efficient, that too in the Radix-2 decimation version. Enough number of zeros are padded to the data in order to convert the length of data to be a power of 2.
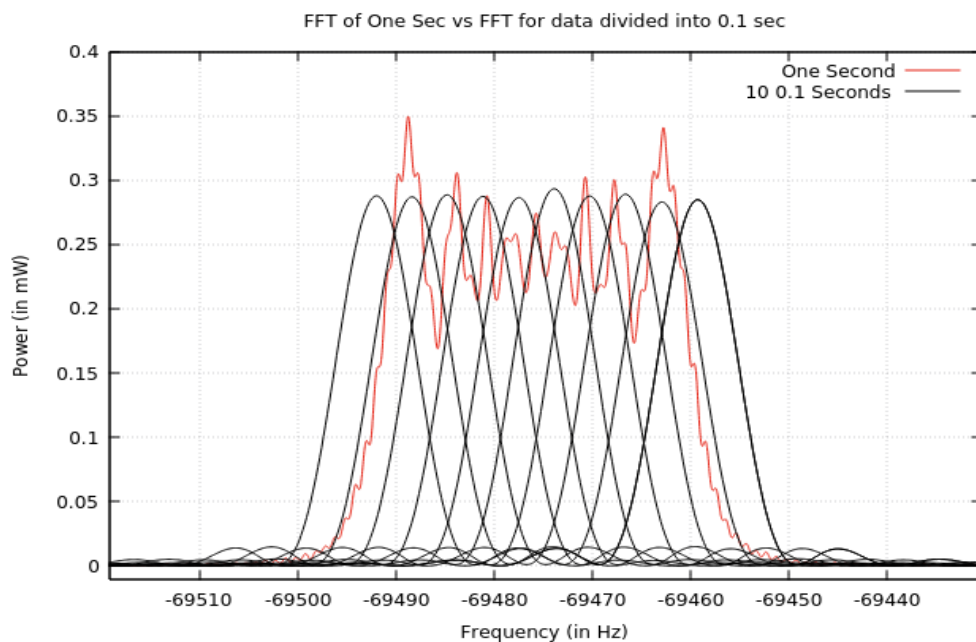
Figure A1-4: FFT for 1 sec vs FFT for ten 0.1 sec data

Initially, one whole second of data (200000 data points) was considered. But since the transmitter and the receiver are in relative motion, Doppler spread was observed as can be seen in Figure A1-4.

In order to solve this issue, the data was divided into smaller windows in the time domain, each section containing about 0.1 sec of data. But it only seemed appropriate to choose the number of data points to be a power of 2. Hence the data was sectioned such that each section has a data point of about 2^{14} sample points (nearest power of 2 as 2^{14} corresponds to 0.0819 sec and 2^{15} corresponds to 0.1638 seconds). This aided in improving the time resolution and brought the value closer to the original value.

Initially, the Doppler shift could have been anywhere in the broad spectrum. Now, after time division, the spectrum is converted to a narrow band.

Appendix 2: Windowing

Due to various reasons, while transforming from the time domain to the frequency domain, we can observe spectral leakage, some of which are:

1. Since the data was recorded in an open loop manner (non-periodic capture), sufficient spectral leakage could be expected.

2. The actual FFT assumes that the data it uses is an infinite periodic continuous signal with one period, and thus repeating it will be the exact same signal. But not always will the part of the data be an integral multiplication of the period, this will result in a truncated waveform with different characteristics from the original signal.

3. Also applying no window is like multiplying the data in the time domain with a rectangular window. A rectangular window has a sharp abrupt end on both sides which on translation to frequency domain will introduce leakage to higher frequency components, which will again, contribute to spectral leakage.

This can be reduced by using a window with smooth ends. Hence to remove the spectral leakage two different commonly used windowing methods were tested. Namely, Hanning window and Hamming window, which aided in increasing the spectral accuracy.

A2.1. Rectangular Window

Fourier transform of a rectangular window is square of sinc function $(\sin(x)/x)$. The side-lobes for rectangular window decays rather slowly causing aliasing effect. The Rectangular window in the time domain and frequency domain are as shown in Figure A2-1.
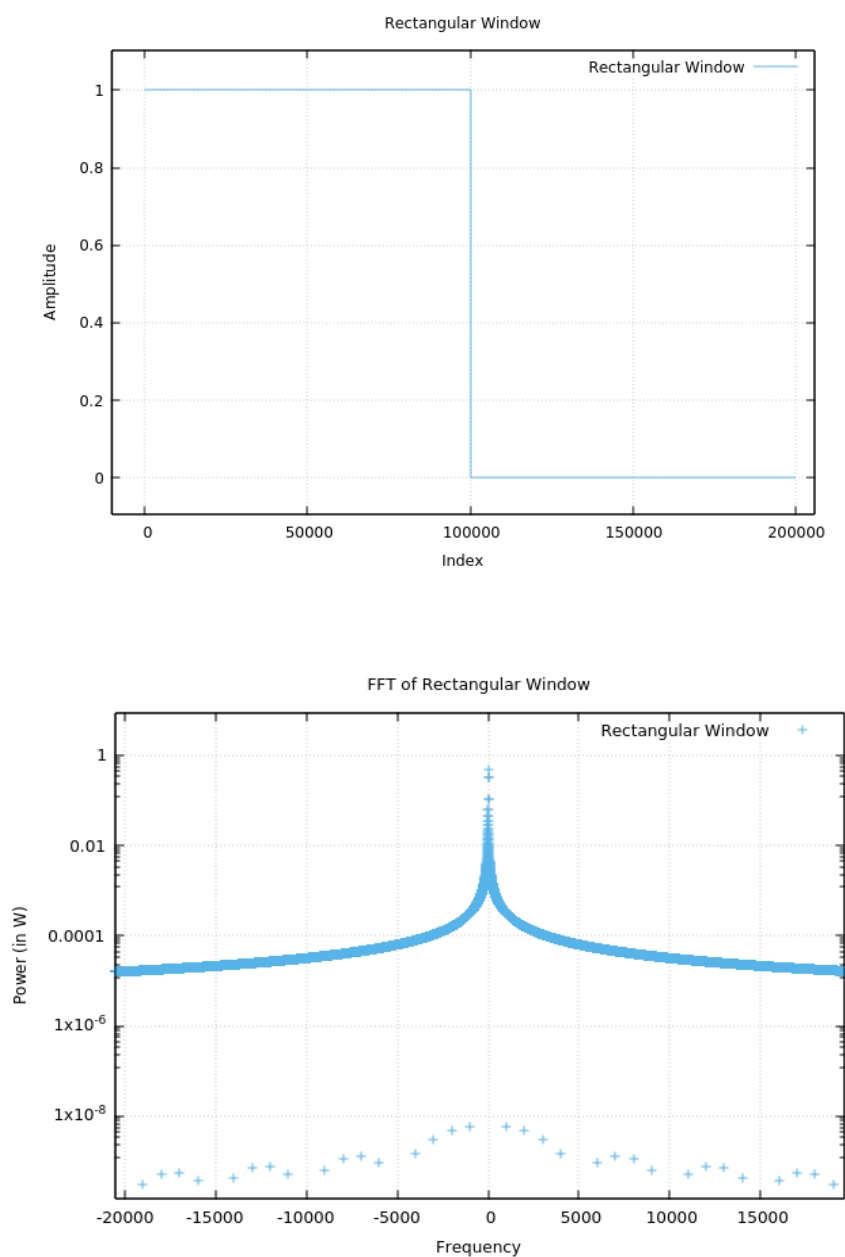
Figure A2-1: Rectangular Window

A2.2 Hamming Window:

Hamming window is a raised cosine window and has end-points slightly raised than zero. The window is expressed as

$$w[n] = 0.5 \left[1 - \cos \left(\frac{2\pi n}{N} \right) \right] = \sin^2 \left(\frac{\pi n}{N} \right)$$

The Hamming window in time domain and frequency domain are as shown in Figures A2-2 (a) and (b). As we can see from Figure A2-1 and Figure A2-2, the attenuation in side lobes of the Hamming window is high compared to that in the rectangular window.
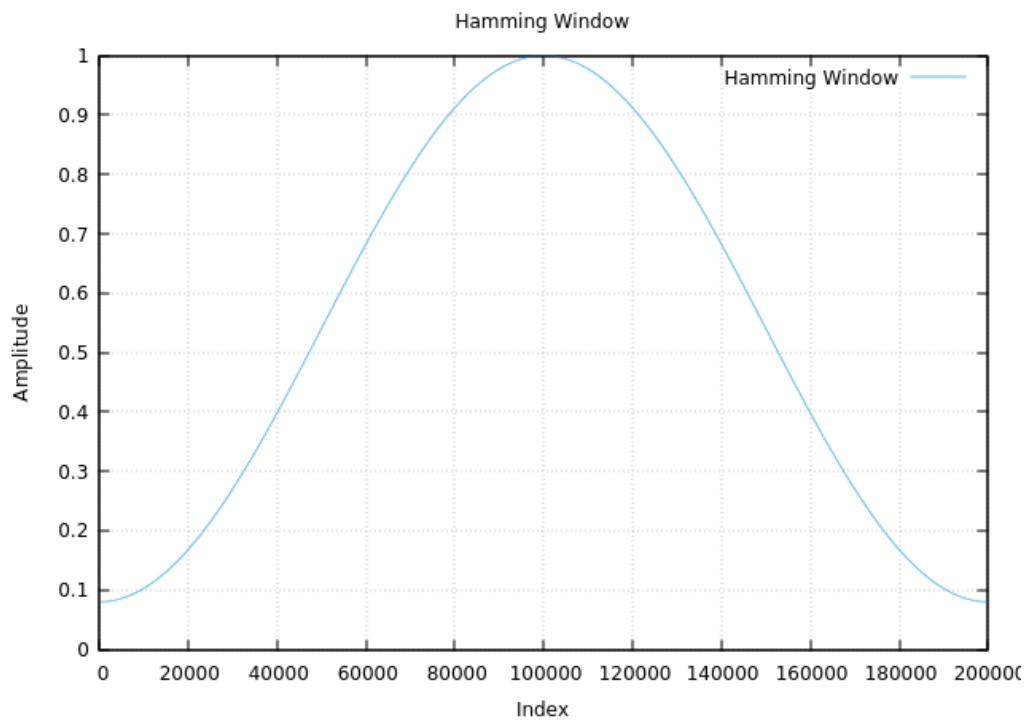
Figure A2-2(a): Hamming Window in time domain
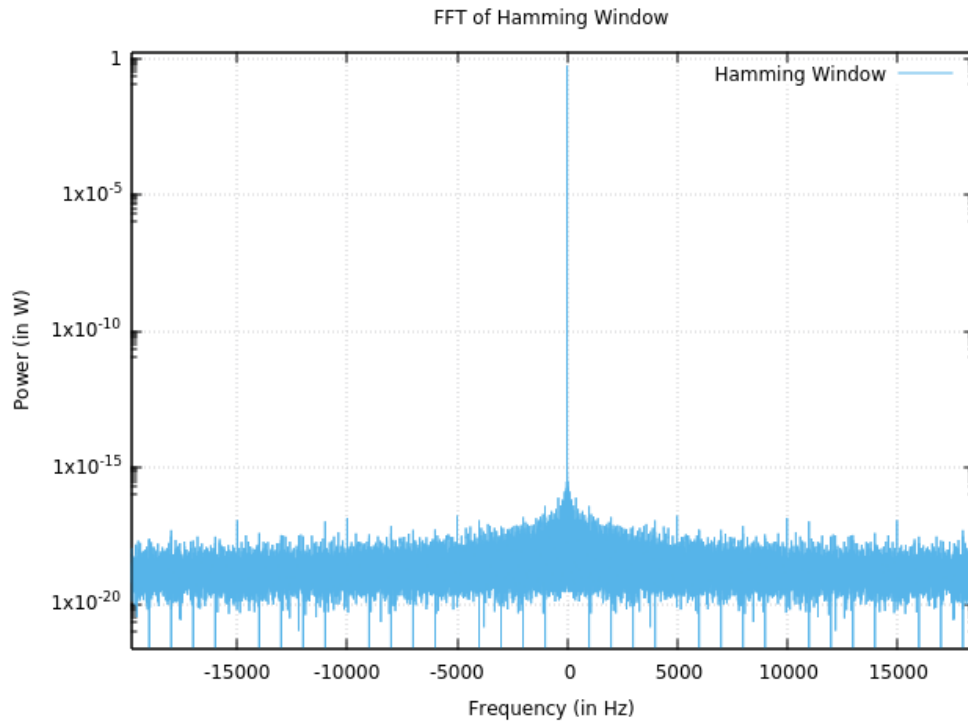
Figure A2-2(b): Hamming Window in frequency domain

A2.3. Hanning window

Hanning window is a raised cosine window and has end-points slightly raised than zero. The window is expressed as

$$w[n] = 0.5 \left[1 - \cos\left(\frac{2\pi n}{N} \right) \right] = \sin^2\left(\frac{\pi n}{N} \right)$$

The Hanning window in the time domain and frequency domain are as shown in Figures A2-3(a) and A2-3(b).
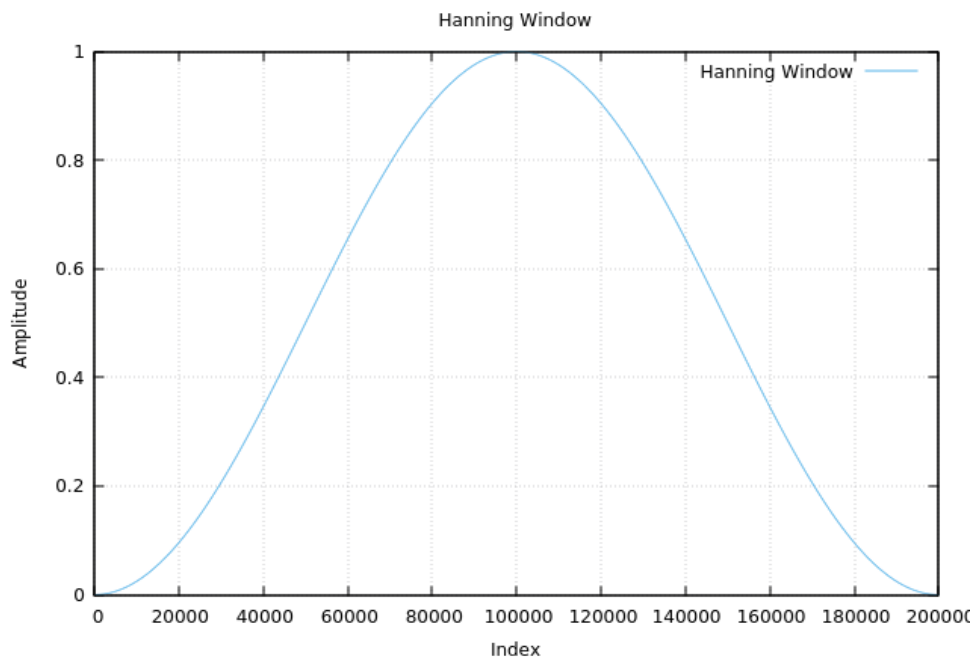
Figure A2-3(a): Hanning Window in time domain

A2.4: Window Correction

Figure A2-4 shows a comparison of power output after the application of three types of windowing. From this figure, it can be seen that the energy of the signal gets altered depending upon the filter applied. A correction, therefore, is required since energy should be constant even after transformation. Amplitude correction can also be applied when frequency precision is required. Frequency correction can also be applied if amplitude precision is required. But both corrections however cannot be applied simultaneously. Thus depending on the application one needs to choose the correction which is to be applied. As the main focus of the current problem is the frequency precision, an energy correction of 1.63 is applied to a hamming windowed signal and a correction of 2.0 is applied to a Hanning windowed signal.
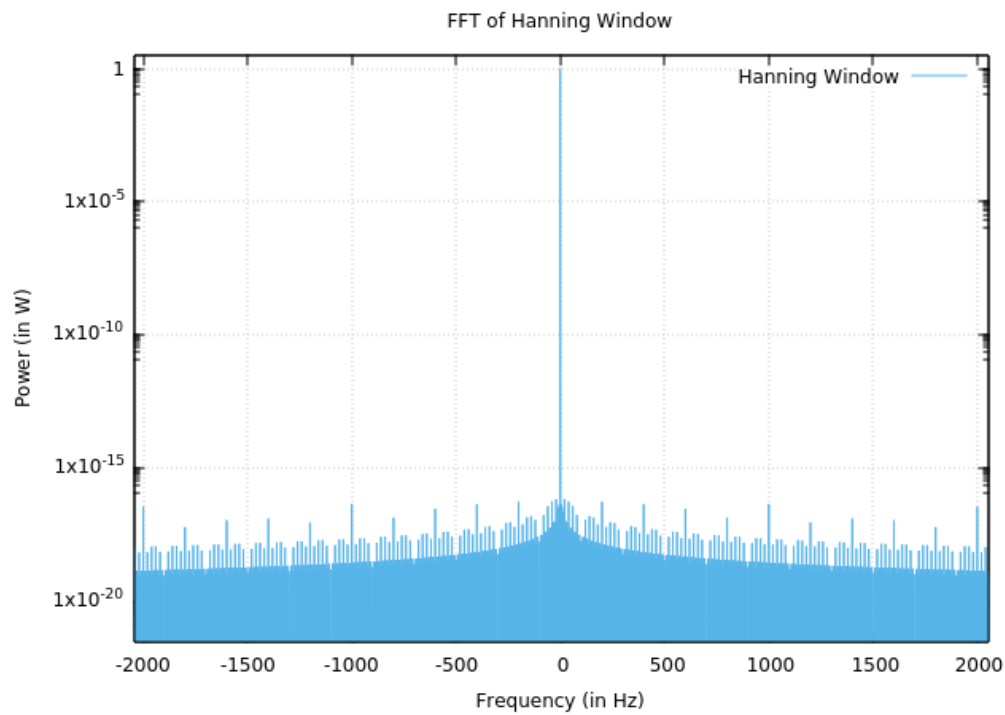
Figure A2-3(b): Hanning Window in frequency domain

The corrections to be applied for the windows under consideration are:

Window	Amplitude Correction Factor	Energy Correction Factor
Rectangular	1.00	1.00
Hamming	1.85	1.69
Hanning	2.00	1.63

Table A2.1: Comparison between different windowing techniques after energy correction.
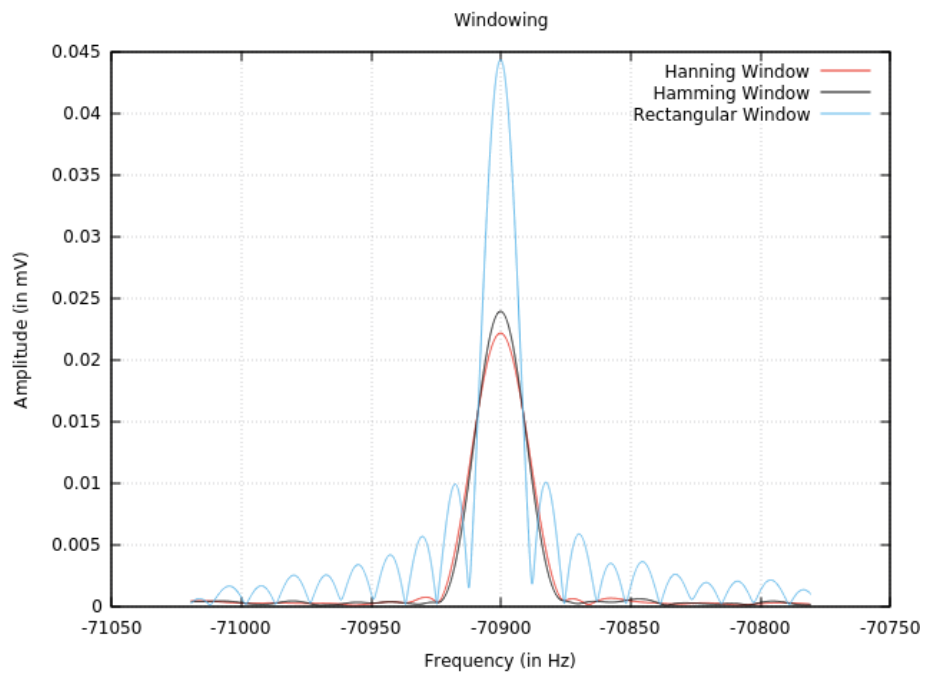
Figure A2-4: Windowed Signal (zoomed in on peak)
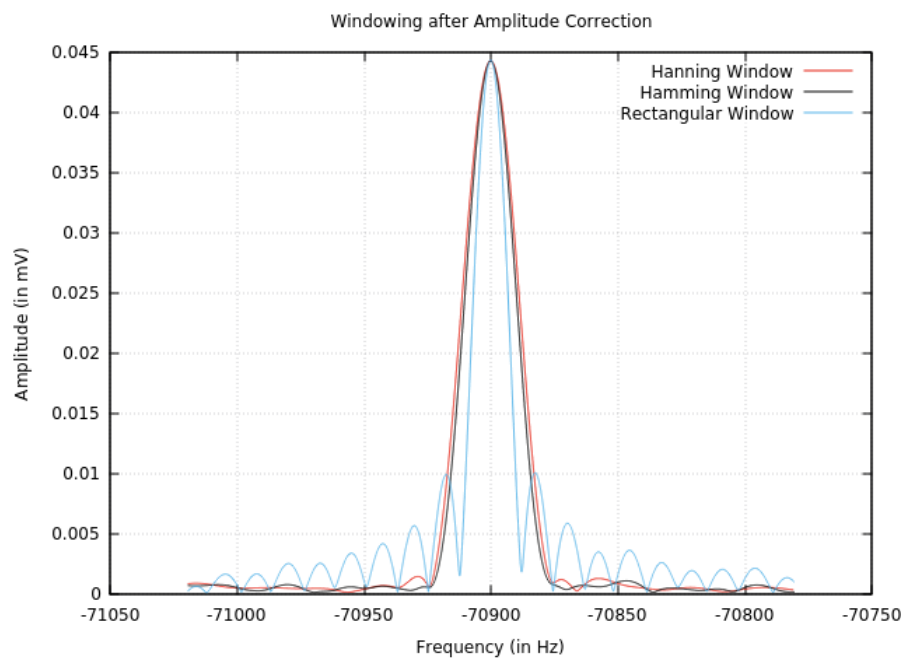
Figure A2-5: Windowed signal after Amplitude Correction (zoomed in on peak)

As can be seen from Figure A2-6(a), when a signal is captured periodically, on repetition, the reconstructed signal will look exactly like the original signal. But when it is not captured in a periodic manner, as shown in Figure A2-6(b), the repetition does not resemble the original signal.

For different, types of signals, different types of windows are optimum. Since the experimental signal is aperiodic, and FFT always assumes that the signal to periodic, the assumed input signal will be different as compared to the actual input. This could result in a spectrum which is different from that of the original signal. Since the Hanning window, which has tapered ends ending and starting at zero, when applied, the repetitions appear to be continuous rather than having an abrupt jump.
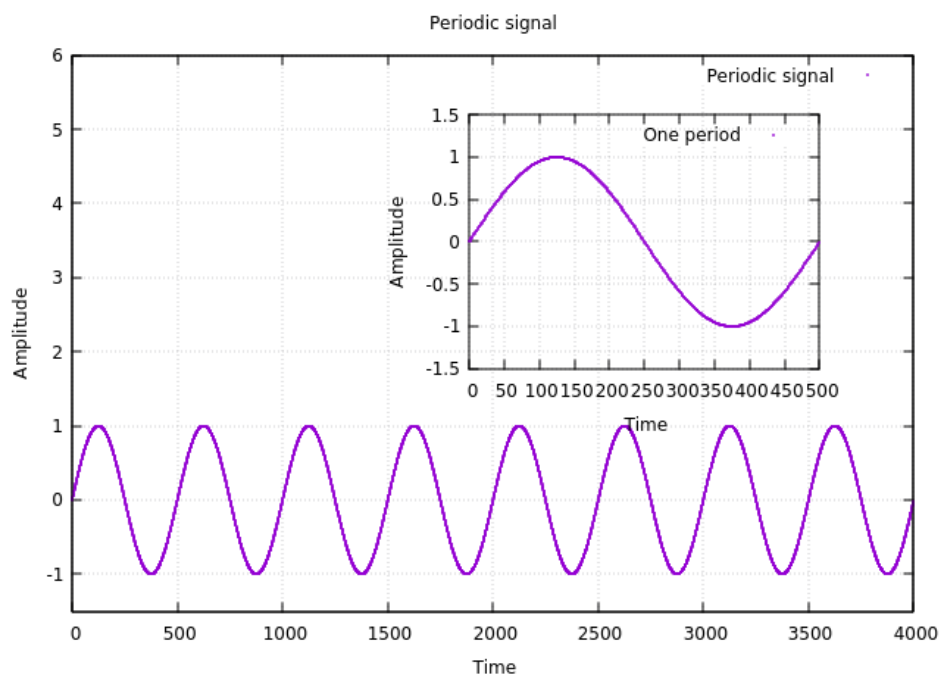
Figure A2-6(a): Periodically captured signal
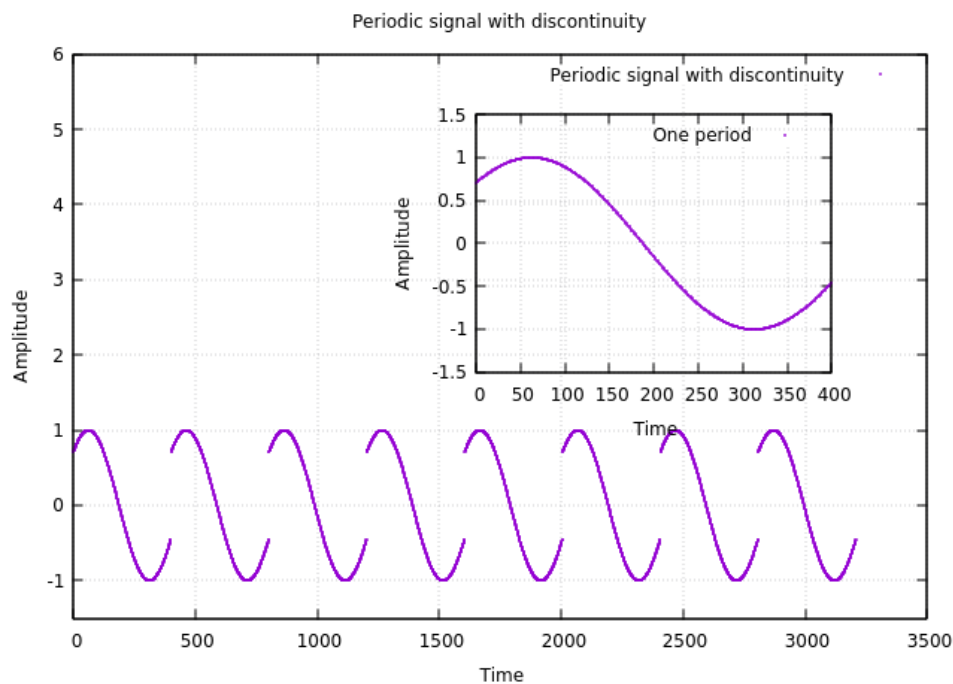
Figure A2-6(b): Aperiodically captured signal

Since our signal is a sine-wave and a combination of sine-waves and is captured aperiodically, Hanning window with an energy correction is used for the analysis of this data.

Appendix 3: Heterodyning

Heterodyning is the process of mixing two signals in order to obtain a combination of signals with the sum and difference of the frequencies.

If the signal frequency variation is too broad, filtering may not be effective as an all-pass filter will have to be applied. Hence to implement low pass narrow-band filtering, data is heterodyned with a signal with predicted frequency. The predicted frequency is calculated using the position and velocity information of the transmitter and receiver which will be discussed in detail in subsequent sections.
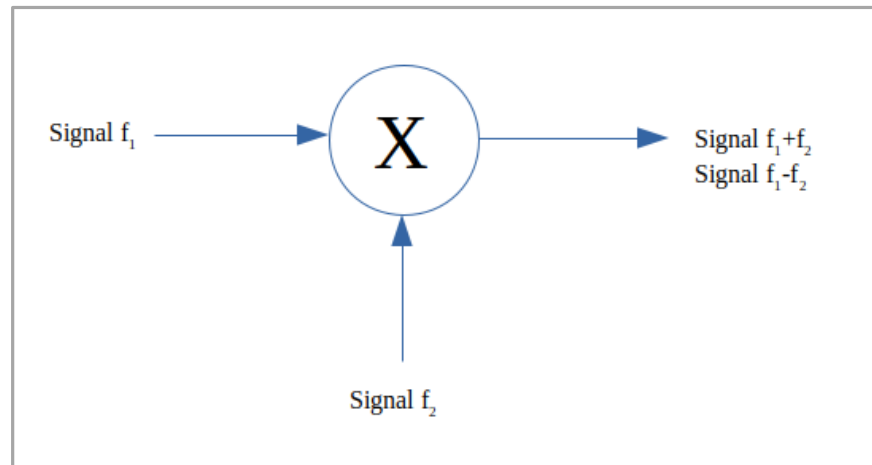
Figure A3-1: Heterodyning Principle

Once the frequency is obtained, a pure carrier signal is generated using the complex exponential function.
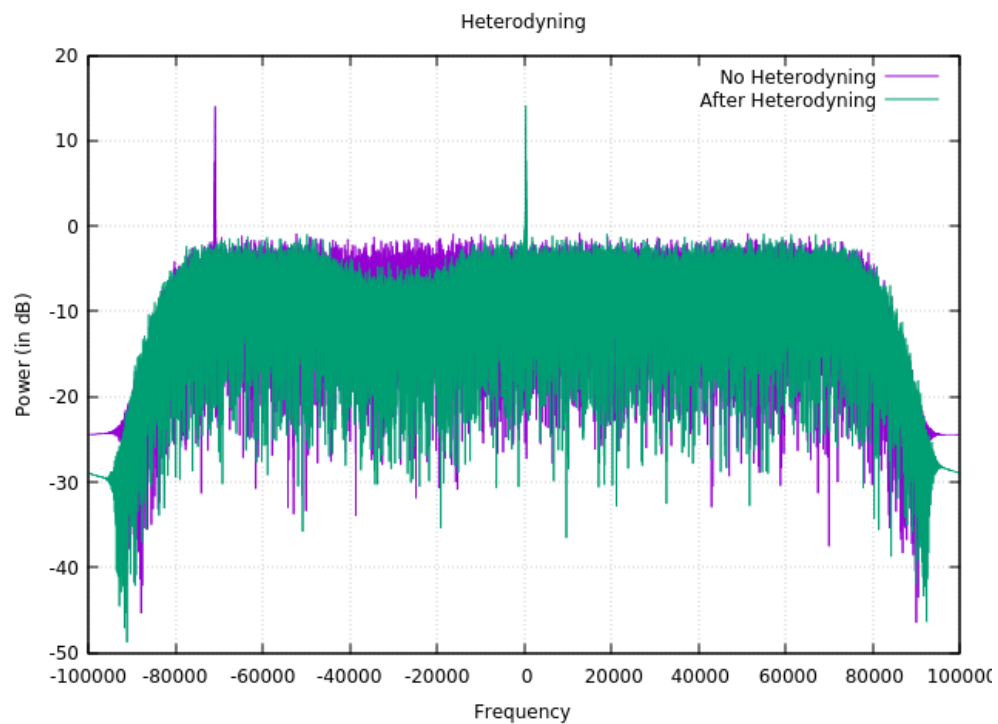
Figure A3-2: Output after heterodyning

Appendix 4: Low pass filtering

In order to remove high-frequency fluctuations, a low pass digital filter is applied with an upper cut off frequency of 4kHz, as the shift due to the atmosphere of the planet under consideration near the surface was observed to be around 3.5kHz.
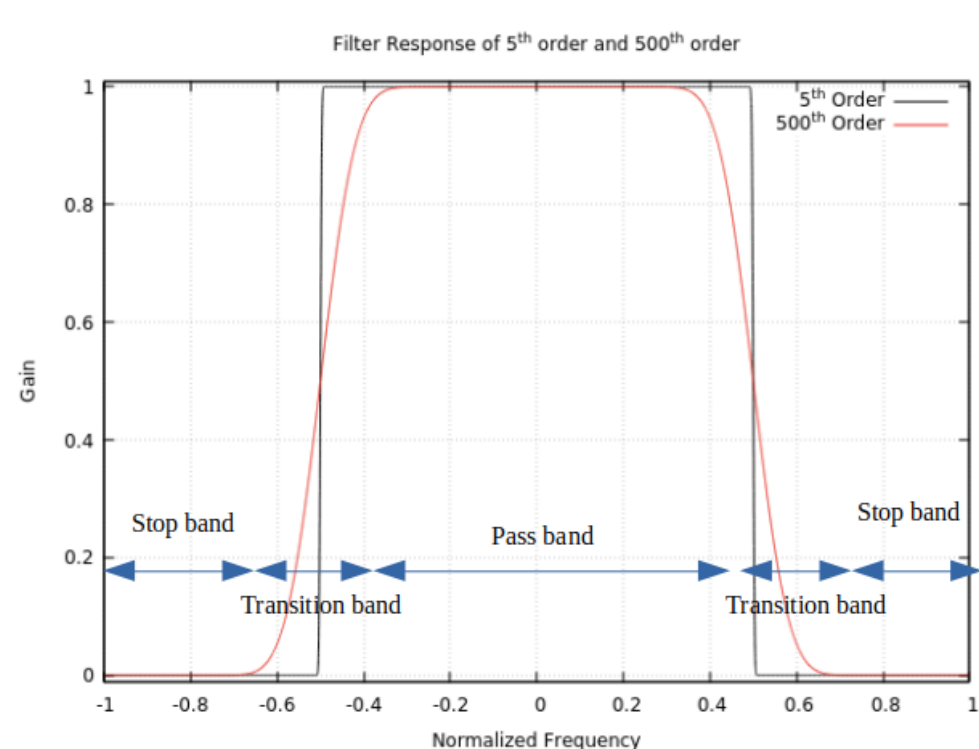

Figure A4-1: Low Pass Filter Response of 5th and 500th order

Ideally, in a filter right after the pass-band, comes the stop band without a transition band. But practically, it is not so. A transition band exists between the two. Higher order filter implies narrow transition band, as can be seen from Figure A4-1, thus providing better amplitude preservation in the pass-band. It can also be seen that higher the order better the filter. But care must be taken to balance the trade off between the quality of filtering and cost of filtering. After sufficient trials, it is observed that the filter of order greater than 10 works fine. Hence, the order of filter chosen is 10.
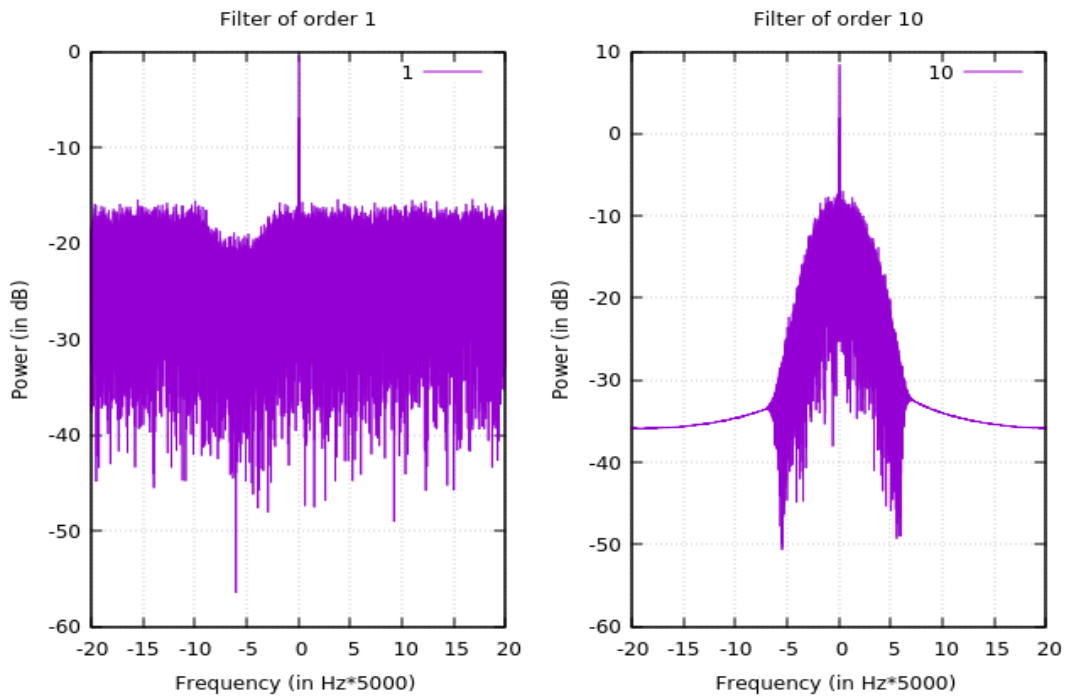
Figure A4-2: Filter of Different Orders (1st and 10th order)

Appendix 5: Doppler Resolution

In the extraction of Doppler shift a frequency resolution of at-least 0.005Hz is required because the shift due planetary atmosphere/ionosphere is of the order 0.01Hz or less. Resolution is given by

$$Res = f_{s1}/N,$$

where f_{s1} is sampling rate and N is the number of frequency bins. The number of frequency bins is nothing but equal to the number of data points considered for FFT. For the DFRS data set the resolution will be 12.207031 Hz, which is very poor as f_{s1} is 200kHz and N is 2^{14}.

Better resolution is obtained when the resolution value is small. This can be achieved by either reducing either f_{s1} or increasing N. Decreasing f_{s1} can be obtained by down-converting the signal. But according to Nyquist, the sampling frequency should be atleast twice the maximum frequency. Here, the maximum frequency is 100kHz and the sampling rate is 200kHz. Hence down conversion is not feasible at all.

The other option is to increase the number of frequency bins in the frequency domain. This can be achieved by padding a required number of zeros without affecting the spectrum. In order to make the resolution to be around $0.005 N$ is made to be 2^{25}.

Appendix 6: Fitting

In order to improve the resolution of frequency further to improve accuracy, the peak is extracted and a curve fitting is carried out with different curves namely, Polynomial fit, Sinc^2 fit and spline fit. The fitting is done on the peak of the power spectrum. The numbers of points taken for each fitting are varied, mainly because as we vary the number of points taken, the shape of the peak changes from a straight line to a polynomial to a Sinc.

A6.1: Polynomial Fit

Depending on the nature of the curve, the coefficients of the polynomial of kth order is calculated such that the error between the fitted values and the actual values are minimum. A kth order polynomial is given by :

$$y = a_0 + a_1 x + a_2 x^2 + a_3 x^3 + \dots + a_n x^n + \dots + a_{k-1} x^{k-1} + a_k x^k$$

where x is the independent variable, $a_0, a_1, \dots, a_n, \dots, a_k$ are the coefficients corresponding to n^{th} power of x and y is the dependent variable. Polynomial fitting of different orders ($2^{nd}, 4^{th} \wedge 6^{th}$) were tested.
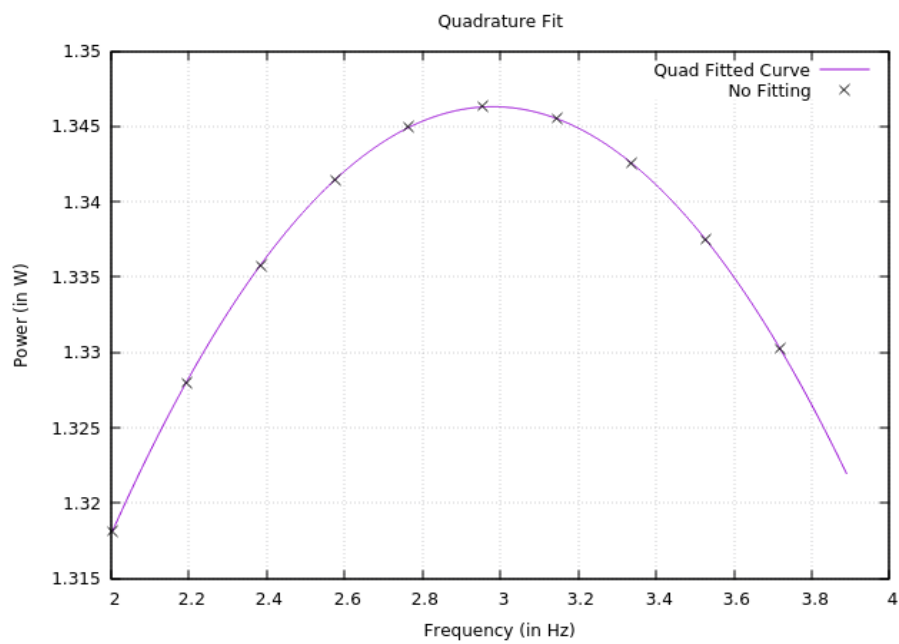
Figure A6-1(a): Quadrature fit
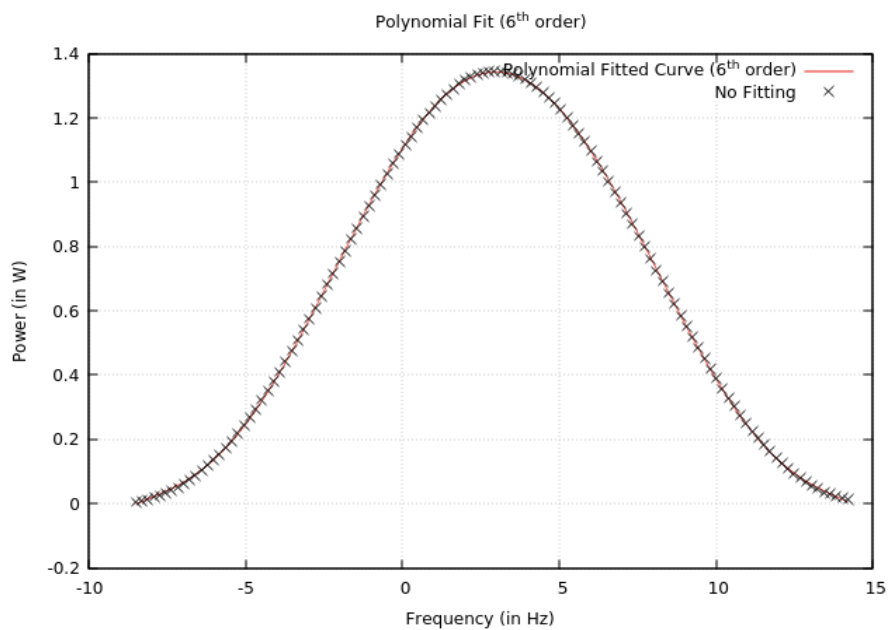
Figure A6-1(b): Fourth and Sixth order Polynomial Fit

A6.2: Sinc² Fit

A power spectrum ideally follows a $sinc^2$ function of frequency (*Lipa and Tyler 1972*) . A $sinc^2$ fit was implemented by optimizing the parameters of sinc function given by

$$y = a * sinc(b(x - c)) + d$$

where, a, b, c and d are the parameters, x the independent variable (here frequency) and y the dependent variable (here power). The parameters are optimized such that the error between the calculated power and the observed power is minimum.
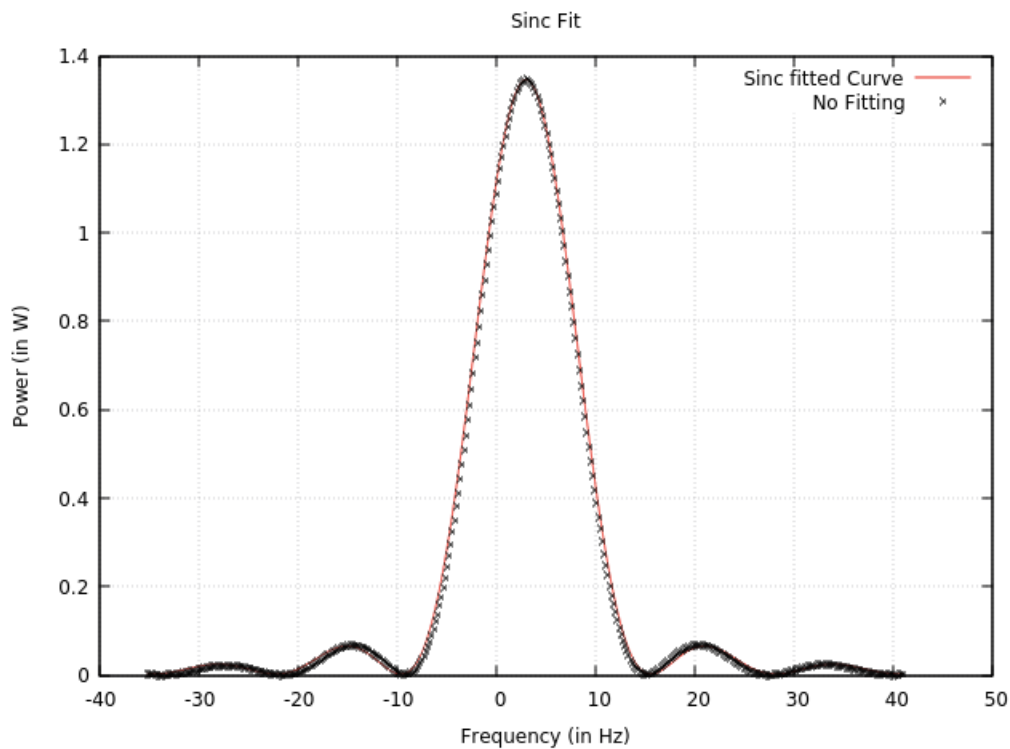

Figure A6-2: $sinc^2$ Fit

A6.3: Spline Fit

Interpolation in Spline Fitting is piece-wise polynomial interpolation. Spline interpolation is preferred as it is known to fit with minimal error even at regions which use lower polynomial.
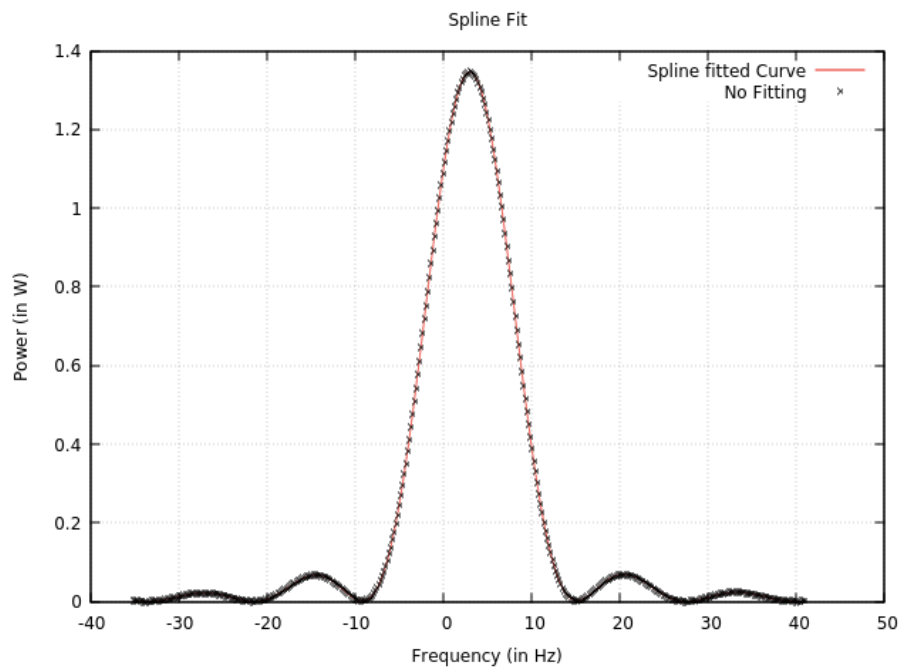
Figure A6-3: Spline Fit

Appendix 7: Residual

From the estimated Doppler shift due to the relative motion of transmitter and receiver at the exact time, and the experimentally obtained Doppler shift, the residual is obtained. This residual contains fluctuations due to the ionospheric plasma and/or atmospheric refractive index.

After a couple of iterations, it was found that at lower resolution of frequencies, quadrature fit gave the best output with less noise. At higher frequency resolution, $\mathrm{sin}c^2$ fitting was functioning with decent results and the results could be seen converging.

From this residual, the electron density of the ionosphere, refractivity, temperature profile and pressure profile of the atmosphere is derived.